CONCENTRATED SOLAR POWER WITH A THERMOCHEMICAL STORAGE SYSTEM

A DIRECT STEAM GENERATION CONCENTRATED SOLAR POWER PLANT WITH A DECALIN/NAPHTHALENE THERMOCHEMICAL STORAGE SYSTEM

By

HAOXIANG LAI, B. Eng.

A Thesis

Submitted to the School of Graduate Studies

in Partial Fulfillment of the Requirements

for the Degree

Master of Applied Science

McMaster University

MASTER OF APPLIED SCIENCE (2017) McMaster University

(Chemical Engineering) Hamilton, Ontario

TITLE: A Direction Steam Generation Concentrate Solar Power Plant with a Decalin/Naphthalene Thermochemical Storage System

AUTHOR: Haoxiang Lai, B. Eng. (McMaster University)

SUPERVISOR: Dr. Thomas A. Adams II

NUMBER OF PAGES: xii, 71

Abstract

This study presents the design and analysis of a new integrated direct steam generation (DSG) concentrated solar power (CSP) plant with a decalin/naphthalene thermochemical storage system. Model simulations were performed in accordance to historical hourly solar radiation data over a year, using a combination of Aspen Plus v10, MATLAB 2016b, and Microsoft Excel VBA. It was found that the proposed plant feasibly stored and discharged energy, based on the solar radiation and chemical storage availability, to maintain base-load power productions (250 MW or 120 MW) with an overall efficiency of 14.6%. The effectiveness of the designed storage system was found to be comparable to a molten salt storage system which is currently used in existing CSP plants. The proposed integrated DSG CSP plant with a decalin/naphthalene thermochemical storage system shows promise for being an alternative to existing CSP plants.

Acknowledgements

First of all, I would like to express my sincere gratitude to my supervisor, Dr. Thomas A. Adams II, for all his support and help towards my master's study. I appreciate very much the freedom, priceless guidance, and helpful suggestions and feedbacks he provides me in all the time of my research and thesis writing. It was truly a privilege to have such a brilliant person as my supervisor for my master's study.

I would like to thank Dr. Chris L. E. Swartz and Dr. Kamil A. Khan for being my examination committee members. I would also like to acknowledge Dr. Vida Meidanshahi (previous student in Dr. Adams' group) with first identifying the decalin/naphthalene chemical reaction pathway as a suitable candidate for CSP applications. Financial support from NSERC Discovery Grant (RGPIN-2016-06310), NSERC Canada Graduate Scholarships-Master's Program, and Ontario Graduate Scholarship Program are gratefully acknowledged.

I would like to express my appreciation to all my colleagues in Dr. Adams' research group and in MACC (McMaster Advanced Control Consortium) for their help and support over the past two years. I would also like to thank Ms. Kristina Trollip, Ms. Michelle Whalen, and Ms. Linda Ellis for their administrative help.

Last but not least, I would like to thank my parents for their endless love, encouragement, and support not only in my academic career but also in my life.

Table of Contents

List of Figures

List of Tables

List of Schemes

List of Abbreviations and Symbols

Abbreviations

TDC	trans-decalin
CDC	cis-decalin
TT	tetralin
NP	naphthalene
PV	photovoltaic
DC	direct current
AC	alternating current
CSP	concentrated solar power
DSG	direct steam generation
PTC	parabolic trough collectors
SPT	solar power towers
LFR	linear Fresnel reflector
PDS	parabolic dish system
HTF	heat transfer fluid
TES	thermal energy storage
DNI	direct normal irradiance
PSO	particle swarm optimization
VBA	visual basic for applications
HP	high pressure turbine
IP	intermediate pressure turbine
LP	low pressure turbine

Symbols

r, r', r_r, r_r'	reaction rate
w	work
v	vapour fraction
k_s, k_s'	reaction rate constant
K	adsorption equilibrium constant
P	pressure
A	frequency factor
E	activation energy
R	gas constant
T	temperature
H	enthalpy
F	flowrate
W	catalyst weight
η	correction factor
$\dot{V}$	volumetric flowrate
ρ	density
ε	porosity
D	diameter
v	superficial velocity
μ	viscosity
A_{cs}	cross-sectional area
C_p	heat capacity
A	area
β	reaction stoichiometry
$\dot{M}$	mass flowrate
U	overall heat transfer coefficient
h	heat transfer coefficient

N_{tube}	number of tubes
L	reactor length
k	thermal conductivity
Re	Reynolds number
Pr	Prandtl number
α	gas hold up

Declaration of Academic Achievement

Most of the text and figures in Chapter 3 and 4 was included in the paper Lai, H, Adams TA II, A Direct Steam Generation Concentrated Solar Power Plant with a Decalin/Naphthalene Thermochemical Storage System, *Chem Eng Res Design* (submitted August 2017 with a submission number of CHERD-S-17-01375). I performed the research and wrote the paper as lead author.

1. Introduction

Solar energy is an attractive source of renewable energy for electricity production as it is free and emits no direct greenhouse gas emissions. Concentrated solar power (CSP) converts solar radiation to thermal energy, which can then be used to produce power. However, just like the traditional solar photovoltaic (PV) system, CSP suffers from the intermittent nature of sunlight availability and a mismatch between peaks of available solar radiation and electricity demand. The most conventional energy storage system for CSP plants such as molten salt storage system suffers from a small volumetric energy density (~50 kWh m^{-3} of material), limited storage period (due to thermal losses), and high storage temperature (~390°C). In comparison, the thermochemical storage system studied in this work, which has not yet been commercialized, has higher volumetric energy density (~500 kWh m^{-3} of reactant), theoretically unlimited storage period, and ambient storage temperature (Pardo et al., 2014; Peltier & PE, 2014). The challenges of this type of storage systems are the complexity of the reactions involved and the complexity of integration with CSP plants (Pardo et al., 2014).

As the state-of-the-art on thermochemical storage systems, different kinds of reversible reactions have been studied such as metallic hydrides, carbonates system, hydroxides system, redox system, ammonia system and organic system. However, these systems suffer one or more of the following drawbacks: poor

reactivity, poor reversibility, incomplete conversion of reactions, high operating pressure (up to 200 bar), and side reactions (Pardo et al., 2014). To the best of our knowledge, the decalin/naphthalene reaction pair (shown in Scheme 1.1) has not yet been studied as a thermochemical storage system for a CSP plant. However, the lab-scaled reaction kinetics studied by Wang et al. (2008) and Huang and Kang (1995) show that the reactions have high reactivity (under catalyst Pt/γ-Al_2O_3), high reversibility (able to achieve ~100% conversion for both forward and backward reaction), relatively low operating pressure (up to 52 bar), and no side reaction (although reaction intermediates exist) (Huang & Kang, 1995; Wang et al., 2008).

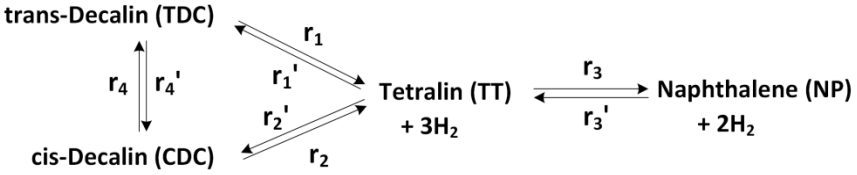

Scheme 1.1. Reversible reactions for the proposed thermochemical storage system. The forward reaction goes from decalin to naphthalene (from left to right), while the backward reaction is from naphthalene to decalin (from right to left).

With the above challenges in mind, this work investigates the feasibility and effectiveness of a direct steam generation concentrated solar power plant with an integrated decalin/naphthalene thermochemical storage system for producing base-load electricity over the course of a typical year in the southern United

States. To the best of our knowledge edge, this is the first time to investigate such a system.

The proposed CSP plant is designed to store the excessive solar energy through the decalin/naphthalene thermochemical storage system while maintaining the base-load power production, when solar radiation is sufficient for base-load power production. As solar radiation diminishes, the storage system discharges energy for maintaining power production on the base-load. With the advantage of high energy density and low storage temperature, the proposed integrated CSP plant and decalin/naphthalene thermochemical storage system is theoretically expected to have higher efficiency and more effective storage than CSP plants with molten salt storage systems.

1.1. Research objectives

In this work, technical feasibility and effectiveness of the integrated DSG CSP plant and decalin/naphthalene thermochemical storage system are investigated by simulating the system in accordance to hourly solar radiation data for an entire year. Furthermore, the designed CSP plant is also compared to an existing CSP plant with a molten salt storage system. Specifically, steady-state base case models are simulated using Aspen Plus v10, reactor models of the thermochemical storage system are developed using MATLAB 2016b, and overall simulations are performed via algorithm developed in Microsoft Excel VBA

by using Excel Aspen Simulation Workbook as an interface to transfer information between models developed in Aspen Plus and MATLAB.

The simulation challenges concentrate on the reactor design and its integration with the designed plant. The reactor is designed to work for both the energy storing step and the energy discharging step, and compatible with both the forward and backward reactions of decalin/naphthalene which are scaled up based on lab-scaled kinetic studies. Besides, the integration of the designed reactor with the plant requires iterative simulations between Aspen Plus and MATLAB to ensure convergence of the integrated model (such as convergence of mass balances), with feasibility analysis of the system and sub-optimization problem of reactor design involved.

2. Literature review

2.1. Concentrated solar power

Global trends of reducing fossil fuel usage and greenhouse gas emissions are the driving forces of utilizing renewable sources of energy such as solar energy. Solar Photovoltaic (PV) and concentrated solar power (CSP) are the two main technologies to capture solar energy for electricity generation. Solar PV has been widely commercialized in industrial scale as well as for residential uses. It converts sunlight directly to electricity and generates DC which commonly needs

to be converted to AC for grid transport. Other than this, the cost of material and required footprint also slows down the development of solar PV for large scale implementations (Labouret & Villoz, 2010). Although large-scaled solar PV plants are currently either in operation or being constructed, the average cost and the future expected cost for PV technologies are higher than those for CSP technologies (Bosetti et al., 2012).

CSP is increasingly gaining attention in the area of power production from renewable sources of energy. Compared to solar PV, the advantages of CSP are relatively lower cost, relatively smaller footprint, and compatibility with thermal storage systems. Hence, CSP is more suitable for large-scale power production (Bosetti et al., 2012; Zhang et al., 2013). The main technologies that are used in CSP plants are parabolic trough collectors (PTC), solar power towers (SPT), linear Fresnel reflector (LFR), and parabolic dish system (PDS) (Zhang et al., 2013). Although they have different configurations, they are all designed to concentrate solar radiation, specifically direct normal irradiance (DNI), by using curved mirrors onto an absorbing tube or a receiver. The concentrated heat is then absorbed by a heat transfer fluid (HTF), which is used to power a steam Rankine cycle for electricity generation (Valenzuela et al., 2004).

Most of the commercial CSP plants are located in Spain and the United States, mainly using PTC technology. Although SPT is implemented in only a small portion of CSP plants, it is gaining increasing interest as it shows higher potential efficiency than the other technologies. Compared to SPT, the advantage of PTC

is low installation cost and low pressure drop. In this study, PTC is chosen since it is mature and widely implemented in CSP plants (Feldhoff, 2012; Valenzuela et al., 2004; Zhang et al., 2013).

The HTF that is used in PTC to carry the solar energy is either oil or steam. When the oil is used, a heat exchanger between the solar field (PTCs) and the power block (turbines) is needed to transfer energy from the oil to secondary steam cycle for power generation (Valenzuela et al., 2004; Zhang et al., 2013). Direct steam generation (DSG) is called when directly using steam as an HTF in the PTC. Compared to oil, the advantages of DSG are non-toxic fluid, higher temperature, no heat exchangers between the solar field and power block, and consequently higher efficiency. However, the drawbacks are two-phase flow (compared to oil which is single phase flow) and higher control effort (Birnbaum et al., 2010; Feldhoff, 2012; Valenzuela et al., 2004).

In this research, DSG CSP with PTC is chosen since it is a mature technology, easy to implement, and also has satisfactory efficiency. To reduce the simulation complexity of the proposed integrated plant, an overall solar-to-steam efficiency instead of a detailed model is used to represent the solar field. Simulation details can be found in Chapter 3.

2.2. Thermochemical storage system

CSP suffers from the intermittent nature of sunlight and the mismatch between the peaks of sunlight and power demand (as shown in Figure 2.1). A thermal storage system is essential to store the excessive solar energy during the peak of solar radiation and discharge it for power production later in the day when the intensity of sunlight diminishes (Pardo et al., 2014).

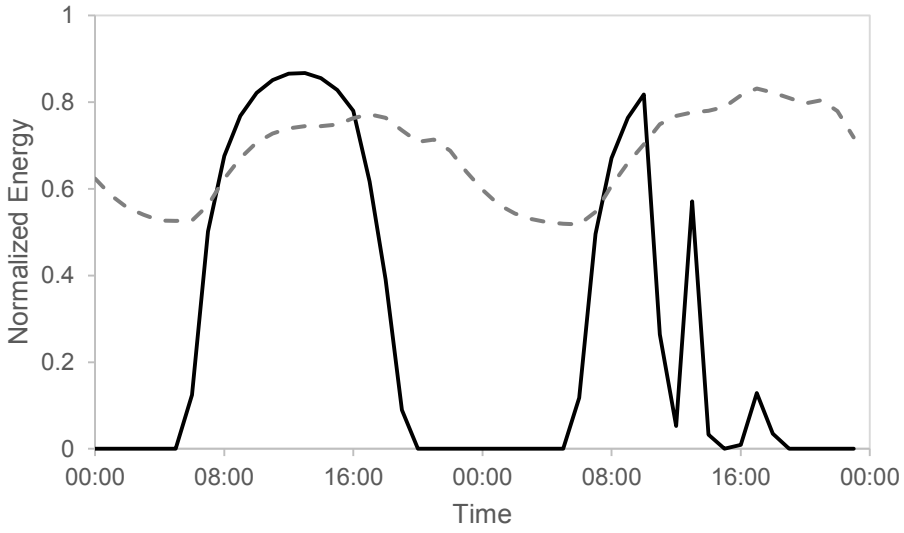

Figure 2.1. Typical profiles of solar radiation and power demand. Solid curve and dash curve represent solar radiation and power demand, respectively.

TES can be cataloged into sensible heat storage systems (such as molten salt), latent heat storage systems (using phase change materials), and thermochemical storage systems (applying reversible chemical reactions). Gil et al. (2010) summarized the required storage materials for the above systems, and Pardo et

al. (2014) summarized the advantages and drawbacks of these systems (Gil et al., 2010; Pardo et al., 2014).

As mentioned earlier, thermochemical storage systems have higher energy density than sensible heat storage systems. Latent heat storage systems have a volumetric density of ~100 kWh m^{-3} of material, which is also lower than thermochemical storage systems. Similar to sensible heat storage systems, latent heat storage systems also typically have limited storage periods and high storage temperatures. Therefore, thermochemical storage systems are expected to have better efficiency than the other two types of storage systems (Pardo et al., 2014).

In terms of technology maturity and complexity, sensible heat storage systems have been implemented in industrial scale and the technology involved is simple (heat exchanger design for heat transfer between HTFs and molten salts). Latent heat storage systems have medium technology complexity involved (phase change of the storage material), which were tested at the pilot scale. The thermochemical storage system is only studied at the laboratory scale and it involves complex technology such as reactor design, heat transfer design, reaction selection and reversibility, and process sizing and optimization (Pardo et al., 2014).

One of the advantages of the thermochemical storage system, when compared to the other types of storage systems, is its capability for long term storage as it has no associated heat loss. However, such a system would require a relatively large

footprint with respect to the solar field (PTCs). This work only focuses on short term storage (aiming at 2-3 hours storage), which can easily be compared to existing CSP plants with different types of storage systems. Moreover, designing a storage system for power production all throughout the day to meet the demand is not considered in this study since it would be taken care of by existing baseline power plants such as nuclear and coal power plants.

2.3. Decalin/naphthalene reactions

As mentioned earlier, decalin/naphthalene reaction pair (shown in Scheme 1.1) is chosen for the thermochemical storage system because of high reactivity and reversibility compared to other chemical reactions that have been studied (Huang & Kang, 1995; Wang et al., 2008). Table 2.1 summarizes the advantages and disadvantages of some of the chemical reaction pairs, that were studied in the literature for the purposes of storing energy, along with the proposed decalin/naphthalene reaction pair (Pardo et al., 2014). As illustrated in the table, the drawbacks of most of the studied chemical reaction pairs concentrate on poor reactivity and reversibility which strongly relate to the effectiveness of the storage system. Poor reactivity and poor heat transfer would result in designing a very large reactor, and low reversibility would lower the system efficiency. Note that, an organic reaction pair, cyclohexane/ benzene, has not been investigated for CSP storage system, but has been studied for chemical heat pump applications.

This pair is similar to the proposed decalin/naphthalene pair in terms of chemical structure, but it has drawbacks such as low reversibility and secondary reaction (Cacciola et al., 1987; Yukitaka Kato et al., 1996).

The advantages of the proposed decalin/naphthalene pair were mentioned earlier with the main disadvantages being the existence of reaction intermediate (TT) and H_2 storage. However, the reaction intermediate (TT) can be avoided (almost zero selectivity to TT in both forward and backward reactions) as observed in lab-scaled kinetic studies (Huang & Kang, 1995; Wang et al., 2008). H_2 storage (or gas phase storage) commonly exists in thermochemical storage systems as can be seen in the table. The current H_2 storage technologies include compressed gas storage, cold compressed storage, liquid H_2 storage, storage via adsorbent (such as MOF-5), storage via liquid organic material, and storage via metal or non-metal hydrides (Sakintuna et al., 2007; U.S. Department of Energy, 2017b). In this study, compressed gas storage is chosen for H_2 storage since it is mature for large scale applications and also because of the ease of computational simulations.

Table 2.1. Advantages and disadvantages of chemical reaction pairs used for thermochemical storage systems in literature.

Reaction	Advantages	Disadvantages	References
MgH_2/Mg	. High reaction reversibility . No by-product . Easy product separation (gas-solid)	. Slow reaction kinetics . High operating pressure (50-100 bar) . Poor heat transfer (solid - wall) . H_2 storage	(Bogdanović et al., 1990; Felderhoff & Bogdanović, 2009)
$CaO/CaCO_3$	. No catalyst needed . No by-product . Easy product separation (gas-solid)	. Poor reactivity . Agglomeration and sintering . CO_2 storage	(Badie et al., 1980; Kyaw, Kanamori, et al., 1996; Kyaw, Matsuda, et al., 1996; Meier et al., 2004; Stanmore & Gilot, 2005)
$MgO/Mg(OH)_2$	. No catalyst needed . Low operating pressure (1 bar) . Good reaction reversibility	. Poor reactivity . Low thermal conductivity	(Ervin, 1977; Y. Kato et al., 1999; Yukitaka Kato et al., 1996, 2001, 2009)
BaO/BaO_2	. No catalyst needed . No by-product . Low operating pressure (0-10 bar)	. Incomplete conversion of both the forward and backward reactions	(Bowrey & Jutsen, 1978; Fahim & Ford, 1983)
NH_4HSO_4/NH_3	. No catalyst needed . Easy product	. Corrosive products ($S0_3$) . Toxic products	(Garg et al., 1985; Wentworth & Chen, 1976)

	separation (gas-liquid)	. No experiment feedback	
$NH_3/N_2 – H_2$	. Well known ammoniac synthesis . No by-product	. Incomplete conversion of both the forward and backward reactions . H_2 and N_2 storage	(Carden, 1977; Garg HP et al., 1985; Kreetz et al., 2000; Kreetz & Lovegrove, 1999; K. Lovegrove, 1993; K Lovegrove et al., 2004; Keith Lovegrove et al., 1999)
CH_4/CO_2	. High reaction enthalpy (~ 250 kJ mol^{-1}) . Industrial feedback	. Side reactions . Low reversibility . H_2 storage	(Edwards et al., 1996; Fedders et al., 1975; Fedders & Höhlein, 1982; Wörner & Tamme, 1998)
C_6H_{12}/C_6H_6	. Industrial feedback	. Secondary reaction . Low reversibility . H_2 storage	(Aristov et al., 1993; Cacciola et al., 1987; Garg HP et al., 1985)
$C_{10}H_{18}/C_{10}H_8$ (decalin/ naphthalene)	. High reaction conversion . High reaction reversibility . No side reaction	. Reaction intermediate exists . H_2 storage	(Hodoshima et al., 2003; Huang & Kang, 1995; Rahimpour et al., 2011b; Sebastián et al., 2008; Wang et al., 2008)

Although the proposed decalin/naphthalene reaction pair has not been investigated as a thermochemical storage system for a CSP plant, its applications on hydrogen production and storage can be found in the literature (Hodoshima et al., 2003, 2005; Sebastián et al., 2008). Besides model simulation studies on the forward reaction (decalin dehydrogenation) coupled with Fischer-Tropsch synthesis for hydrogen production can also be found (Rahimpour et al., 2011b, 2011a).

Wang et al. (2008) had studied the gas phase forward reaction kinetics at the lab scale, between a temperature range of 250 – 350°C at atmospheric pressure using Pt/γ-Al_2O_3 catalyst. This study focused on the developing the reaction rate equations and the estimation of the associated parameters over the above-mentioned temperature range. The study showed that at least 95% conversion of decalin (TDC and CDC) could be achieved with almost 100% selectivity to NP over TT (the intermediate) (Wang et al., 2008).

Huang and Kang (1995) had experimentally studied the backward reaction kinetics using Pt/γ-Al_2O_3 catalyst for a temperature and pressure range of 200 – 260°C and 17.2 – 86.2 bar respectively. Under these conditions, TDC, CDC, TT, and NP are in the liquid phase while H_2 is in the gas phase. The study found that the reaction conversion of NP is very close to 100% under various conditions. The selectivity to TDC and CDC varied with temperature and pressure, but the

selectivity to TDC was always higher than CDC as expected (Huang & Kang, 1995).

2.4. Existing CSP plants with storage systems

Table 2.2 summarizes some of the existing or developing CSP plants with storage systems in the world. As shown in the table, the molten salt storage system is currently the most mature storage technology for CSP plants. It has been implemented in CSP plants for years and is expanding its implementation towards future development. In this study, the proposed CSP plant with a decalin/naphthalene thermochemical storage system is designed to have the same power output and aperture area of PTC similar to the Solana Generating station for the ease of comparison, since Solana Generating Station is the largest known CSP plant in operation with the molten salt storage system. A detailed design can be found in Chapter 3. Based on the advantages and disadvantages discussed earlier in this chapter, the designed first-known DSG CSP plant with an integrated decalin/naphthalene thermochemical storage system proposed in this work is theoretically a better option than CSP plants with molten salt storage systems, which was the motivation of this study.

Table 2.2. Summary of some of the existing and developing CSP plants with storage systems in the world.

Plant	Location	Power output	Solar field	Storage	Start date	References
Solana Generating Station	Arizona, U.S.	250 MW	PTC	Molten salt	October, 2013	(Abengoa Solar, 2013; Peltier & PE, 2014)
Crescent Dunes Solar Energy Project	Nevada, U.S.	110 MW	SPT	Molten salt	November, 2015	(NREL, 2016b; U.S. Department of Energy, 2014)
Ouarzazate Solar Power Station (NOOR I)	Ouarzazate, Morocco	146 MW	PTC	Molten salt	December, 2015	(NREL, 2017a)
Rice Solar Energy Project	California, U.S.	150 MW	SPT	Molten salt	January, 2016	(NREL, 2013; Zhang et al., 2013)
Xina Solar One	Pofadder, South Africa	100 MW	PTC	Molten salt	2017	(NREL, 2015a)
Delingha	Delingha, China	50 MW	PTC	Molten salt	2017	(NREL, 2017b)
Atacama - 1	Calama, Chile	110 MW	SPT	Molten salt	June, 2018	(NREL, 2015b)
Golmud	Golmud, China	200 MW	SPT	Molten salt	July, 2018	(NREL, 2016a)
Kathu Solar Park	Kathu, South Africa	100 MW	PTC	Molten salt	2018	(NREL, 2016c)
TuNur	Rjim Maatoug, Tunisia	2.5 GW	SPT	Molten salt	Developing	(Nur Energie Ltd., 2010)

3. Process Modelling

3.1. Process Overview

The proposed CSP plant consists of three main components: a solar field filled with parabolic troughs, a thermochemical storage system, and a power block (Figure 3.1). The system was designed to be switchable between different operating modes based on the overall strategy shown in Figure 3.2. When solar radiation is high enough to exceed the base-load electricity production, it operates in storage mode. In this mode, water is pumped from the water tank to the solar field, gets heated through the parabolic troughs and forms superheated steam. A portion of the steam expands through the turbines and generates electricity, which completes a steam Rankine cycle. The resulting low pressure steam is then condensed and returned to the water tank. The remaining portion of steam flows through the tube side of the reactor, condensing and providing heat for the shell side where an endothermic reaction takes place. As shown in Scheme 1.1, decalin reacts to form naphthalene and hydrogen gas as final products. The excessive energy that the steam carries from sunlight is then stored in the form of chemical potential. The resulting water still has a relatively high temperature. Instead of returning to the water tank, it joins the inlet water to the solar field for the purpose of saving waste heat. The storage mode was

designed for two different base-loads of power production (250 MW and 120 MW) depending on the solar radiation availability.

As the solar radiation diminishes, the discharge mode takes over. Water flows from the water tank to the tube side of the reactor and absorbs heat from the reverse reaction. Naphthalene reacts with hydrogen reversely to form decalin, which is an exothermic reaction. Heat is released from the reaction to vaporize water and superheat the resulting steam. By feeding the steam to the power block, electricity is generated. The power block is capable of bypassing the inlet steam to reheat the steam between each turbine for higher efficiency.

The third operating mode, transient mode, is active when sunlight is present but insufficient to maintain the second base-load power production (120 MW). It is a combination of storage and discharge mode, such that the water flowing from the water tank enters both the solar field and the reactor. A portion of water gets energy from the sunlight, while the other portion is heated up by the reversed reaction. The additional energy discharged from the storage system compensates the insufficient solar energy to keep a base-load power production.

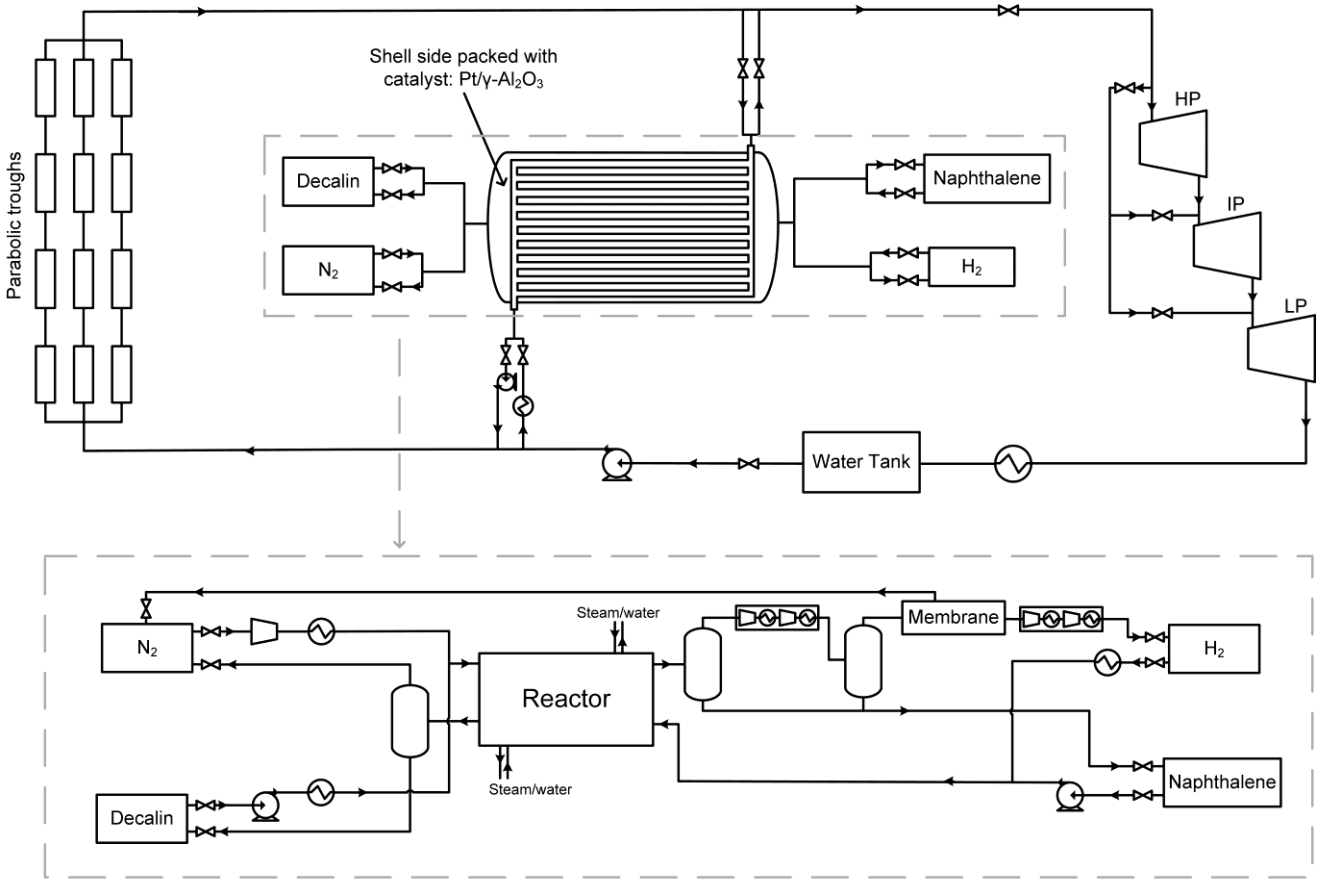

Figure 3.1. Scheme of the overall Concentrated Power Plant (CSP) with detailed scheme of the storage system.

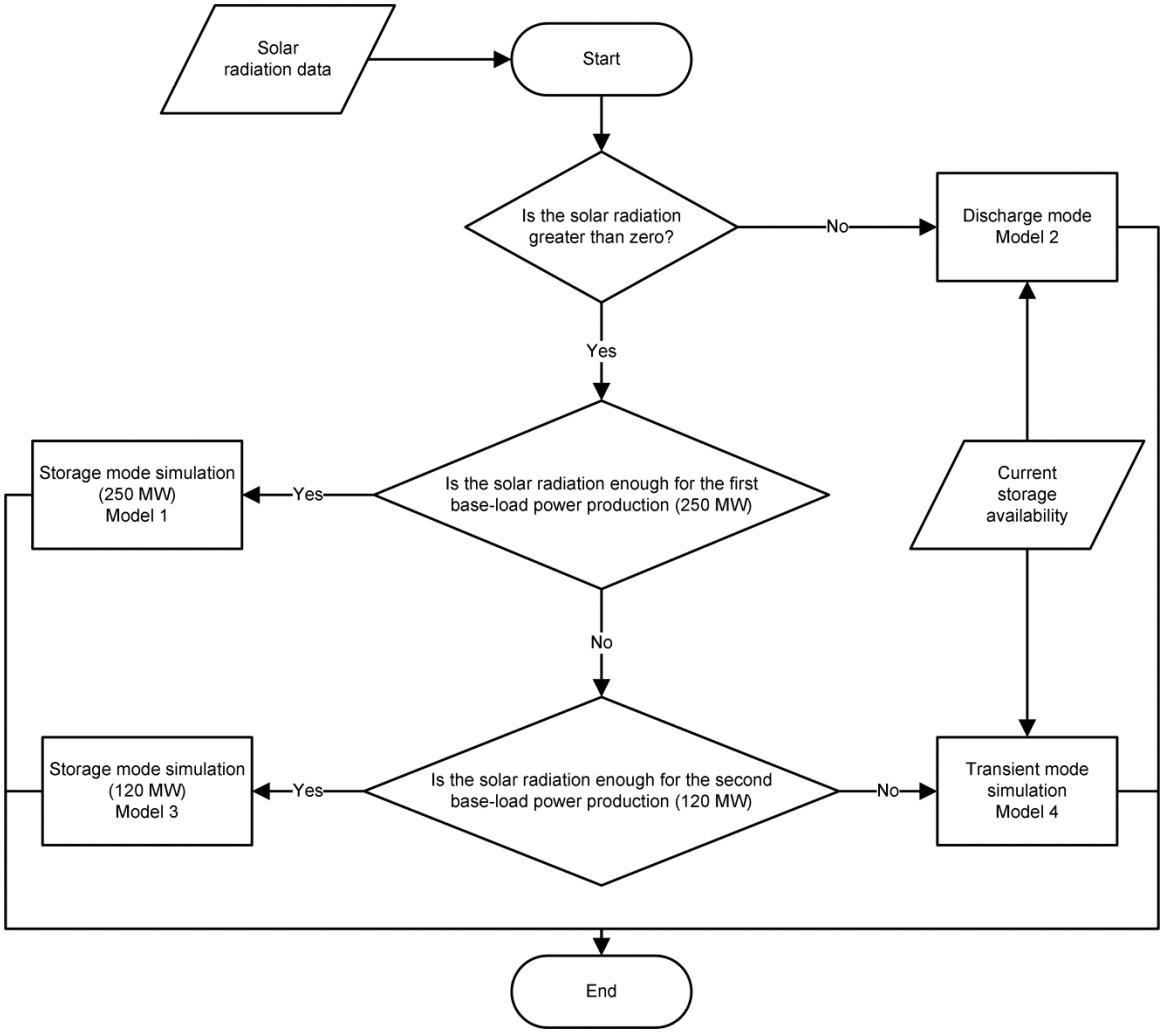

Figure 3.2. Overall strategy of switching the proposed CSP plant between different operating modes.

The objective of modelling and simulating the CSP plant is to obtain electricity production profiles according to the solar radiation profiles. To define such a system for simulation, the key design parameters and decision variables include water flow rate, operating pressure and temperature of each unit, electricity production, the amount of energy to store or discharge, the amount of reactants

consumed, and sizes of major units. To reduce the degrees of freedom and to compare against a fair standard, the proposed CSP plant was designed similarly to an existing CSP plant which is the Solana Generating Station located in Arizona, US (Abengoa Solar, 2014). The proposed CSP plant has the same total aperture area (of parabolic troughs) as the Solana Generating Station, which is 220 hectare. The power block has a total capacity of 280 MW, also same as the existing CSP plant (Abengoa Solar, 2013). It consists of two sets of turbines. Each set has a total capacity of 140 MW, contributed by a high pressure turbine, an intermediate pressure turbine, and a low pressure turbine. The proposed CSP plant was designed to produce power on base-loads of either 250 MW or 120 MW by running either two full sets of turbines or only one set respectively, depending on the availability of solar energy.

Unlike the molten salt storage system in the Solana Generating Station, the proposed thermochemical storage system consists of several shell-and-tube reactors, pre-heating steps for reactants, and separation processes for products. Steam/water is run on the tube side of the reactors, while reactions take place on the shell side which is packed with catalyst. In CSP, the steam pressure can normally get as high as 100 bar, and hence requires relatively thicker tube walls than the reaction side does (Birnbaum et al., 2010; Valenzuela et al., 2004). Running the steam on the tube side requires only thick tube walls rather than thick tube and shell walls. In terms of storage, Hydrogen and nitrogen are kept in the gas phase, while decalin and naphthalene are stored as a liquid. The forward

reaction happens near atmospheric pressure, while the backward reaction favours high pressure up to 51.7 bar (Huang & Kang, 1995; Wang et al., 2008). Therefore, hydrogen gas is stored at high pressure for use in the backward reaction as well as for reducing the volume of the storage tanks. Nitrogen gas is used as a sweep gas for the forward reaction but is not needed in the backward reaction. The membrane PRISM® PB6050 is used to separate hydrogen from nitrogen in the forward reaction product stream (Air Products, 2017). The desired pressures of both the membrane feed and hydrogen storage are achieved by applying multi-stage compressors. However, because membrane separation is imperfect, some nitrogen is contained within the hydrogen when stored. Decalin has a normal melting point of –30.4°C (trans) or –42.9°C (cis), so there is little risk of freezing at any point of the year in Arizona (Haynes, 2010). However, naphthalene is solid at room temperature since its normal melting point is 80.26°C (Haynes, 2010). In this work, naphthalene is stored above 82°C to avoid solids handling issues.

3.2. Model and Simulation

To model and simulate the proposed CSP plant, we chose historical hourly solar radiation (DNI) data for the location of Solana Generating Station in Arizona from July 2011 to July 2012 as a case study. These data were generated by the Physical Solar Model (PSM) from the National Solar Radiation Data Base

(NSRDB) and is practical to use for simulation purposes since they accounted for different kinds of weather conditions such as rainy days and cloudy days (NREL, 2010). Figure 3.3 summarizes the methodology used to develop the final design, and detailed explanations can be found in the following sections.

3.2.1. Phase 1: Steady-state Base-load Simulations

In phase 1, by assuming 100% conversion of the reaction as well as unlimited amount of chemicals in storage, four base-case models were developed in Aspen Plus v10 with the Peng-Robinson equation of state (EOS) throughout, and STEAM-NBS for steam/water streams. The Peng-Robinson physical property package with default VLE (vapour-liquid equilibrium) parameters gave closest predictions to the experimental results when performing a model validation check on mixtures of decalin, naphthalene, tetralin, hydrogen, and nitrogen (Gao et al., 1999; Miyake et al., 2007; Nasir et al., 1981; Park et al., 1996).

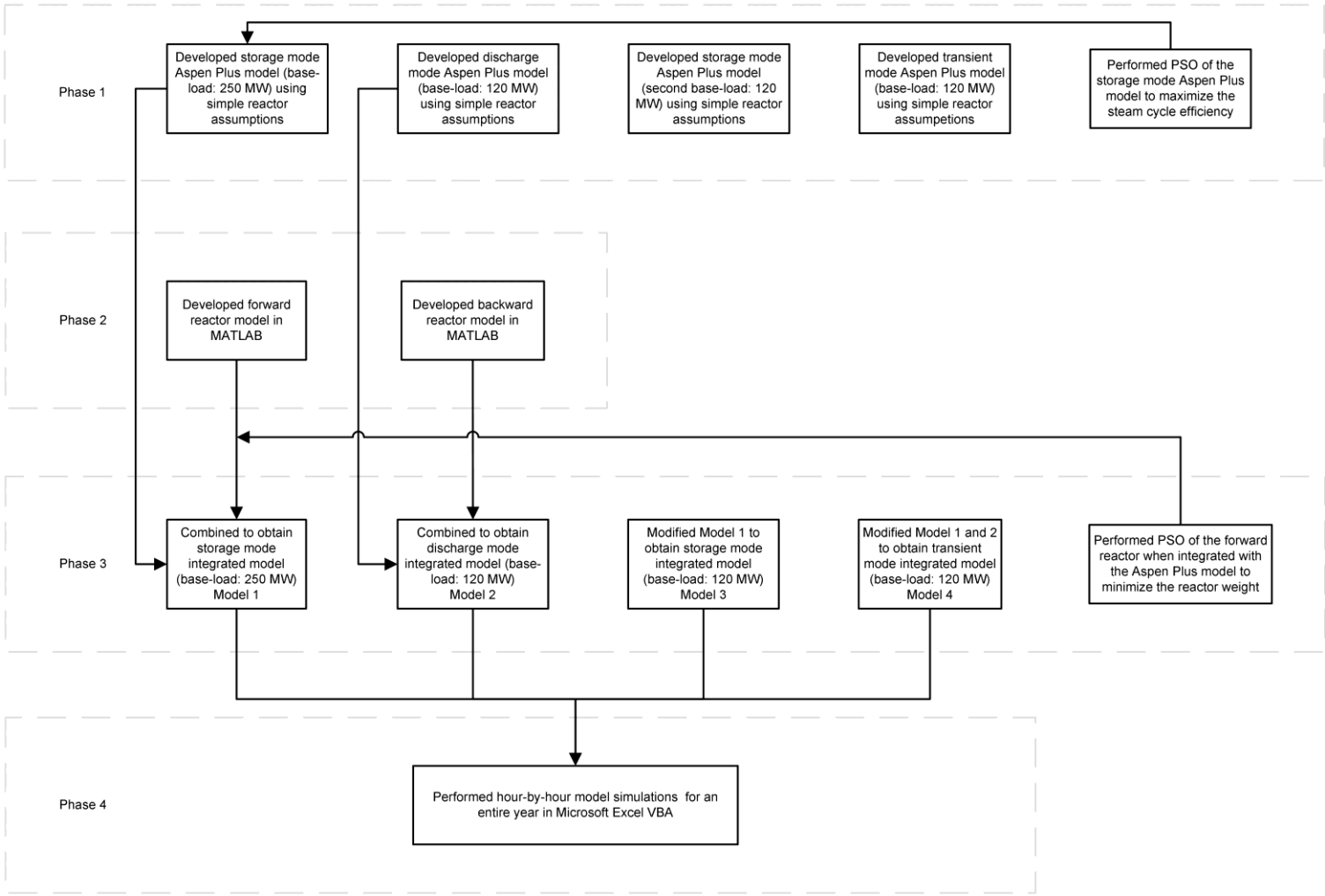

Figure 3.3. Summary of the methodology used to design the proposed CSP plant.

The decalin storage tank was assumed to hold 76% TDC and 24% CDC on a molar basis as this was the inlet concentration to the forward reaction in Wang et al. (2008) (Wang et al., 2008). Due to incomplete membrane separation (recovering only around 78% of H_2 in the feed in the permeate side), the N_2 storage tank contains some H_2 as a result of the recycle and storage of the retentate (Air Products, 2017). After solving the system mass balances, it was found that the H_2 storage tank should contain 79% H_2 and 21% N_2. Pure NP was assumed in the naphthalene tank, which was shown to be a good assumption because the forward reaction can achieve 100% conversion to NP.

The key design parameters used for Aspen Plus model simulations are summarized in Table 3.1. Most of the parameters were taken from references except the turbines' pressures which were determined via particle swarm optimization (PSO). PSO was run on the steam cycle part of the storage mode Aspen Plus model (base-load: 250 MW) to maximize the steam cycle efficiency (defined as the gross electricity production over the total energy input to the system), which is mathematically equivalent to maximizing the gross electricity production when the inlet steam conditions to the HP are fixed. The optimization problem can be formulated as below:

$$max\ w_{HP} + w_{IP} + w_{LP} + w_{pumps} + w_{compressors}$$

$$s.t.\ v_{HP} = 1, v_{IP} = 1, and\ v_{LP} \geq 0.95,$$

where w_i represents the work of each piece of equipment. Pump and compressor work is negative in the above convention. v_i is the outlet vapour fraction (also called steam quality) of each turbine. The decision variables for this optimization were the outlet pressures of the three turbines, and the other design parameters were kept as constant.

Table 3.1. Process design parameters. The asterisk (*) indicates the parameter was a decision variable determined via PSO.

Unit	Key design parameters
Solar field	Outlet temperature: 550°C, outlet pressure: 90 bar, total pressure drop: 10 bar, total radiation-to-steam efficiency: 70% (Birnbaum et al., 2010; Valenzuela et al., 2004)
High pressure turbine	Outlet pressure: 21.5 bar *, isentropic efficiency: 87% (Sanz-Bermejo et al., 2014)
Intermediate pressure turbine	Outlet pressure: 4.7 bar *, isentropic efficiency: 88% (Sanz-Bermejo et al., 2014)
Low pressure turbine	Outlet pressure: 1 bar *, isentropic efficiency: 88% (Sanz-Bermejo et al., 2014)
Reactor	Forward reaction shell side inlet temperature and pressure: 265°C, 2.12 bar; tube side inlet temperature and pressure: 550°C, 90 bar (Birnbaum et al., 2010; Wang et al., 2008)

	Backward reaction shell side inlet temperature and pressure: 400°C, 34.5 bar; tube side inlet temperature and pressure: 285°C, 92 bar (Birnbaum et al., 2010; Huang & Kang, 1995)
PRISM® PB6050 membrane	Inlet pressure: 8.5 bar, permeate pressure: 0.2 bar (Air Products, 2017)
Decalin storage	Temperature: 25°C, pressure: 1 bar
Nitrogen storage	Temperature: 25°C, pressure: 1 bar
Hydrogen storage	Temperature: 25°C, pressure: 35 bar
Naphthalene storage	Temperature: 82°C, pressure: 1 bar

We chose PSO for this optimization problem because it works well for black box models (the Aspen Plus model in this work) and is also parallelizable. Even though it does not guarantee the global optima, it usually gives satisfactory results (Khojasteh Salkuyeh & Adams, 2015). The global optimum is not necessarily needed for this system, as the objective of this study is to analyze the feasibility of the concept with the requirement of finding the best possible design, and because the results of the PSO are used as initial guesses for a later optimization. The PSO code was adapted from previous work of Khojasteh Salkuyeh and Adams (2015) and run in MATLAB 2016b (Khojasteh Salkuyeh & Adams, 2015). The Excel Aspen Simulation Workbook was used as an interface to connect MATLAB to Aspen Plus. The resulting turbine outlet pressures were then used in the other three base-case models since they all had the same steam turbine design.

3.2.2. Phase 2: Reactor Models

The reactor was designed as a shell packed with catalyst and a number of tubes. Counter-current flows of steam/water and reactants run in the tube side and the shell side respectively.

The following assumptions were made when modeling the reactor:

- Steady-state flow
- Negligible radial variations
- Adiabatic reactor (no heat transfer to the surroundings)
- Ideal gas law for all gas-phase species
- Diffusion rates of chemicals to the catalyst surface are much faster than the reactions as assumed in kinetic study of Wang et al. (2008) and Huang and Kang (1995) (Huang & Kang, 1995; Wang et al., 2008)
- Homogeneous model for two-phase flow

A homogeneous model was assumed for two-phase flow region because the computational intensity of applying the flow pattern method for two-phase flow is too large for relatively little gain in the reliability of the simulation results.

The reactor was divided into three stages for simulation purposes in both the forward and backward reaction modes since it involves a phase change region: (1) pre-heating/subcooling, (2) vaporizing/condensing, and (3) super-heating/cooling. The reason to divide into stages is that the equations of physical

properties and energy balances for the tube side (steam/water) are different from stage to stage.

Most of the data for physical property models were retrieved from Aspen Plus V10, and are summarized in Table 3.2. All physical properties of water and steam were taken from NBS/NRC Steam Tables (Haar, 1984). A reduced model of the default equations contained within the Peng-Robinson physical property package was used to estimate pure liquid molar heat capacity for decalin, tetralin, and naphthalene in the backward reaction. Mixture heat capacity was estimated by the average heat capacity of each component on a molar basis. The estimated properties were validated with predictions from Aspen Plus using the Peng-Robinson package with less than 1% error. By assuming a homogeneous model for two-phase flow, the mixture properties were calculated as the volume-average of properties of each component.

The reaction kinetics are based on lab-scale kinetic studies by Wang et al. (2008) and Huang and Kang (1995) for the forward reaction and backward reaction respectively. Although both the forward reaction and backward reaction use the same catalyst Pt/γ-Al_2O_3, they were studied under different conditions. Wang et al. (2008) studied the forward reaction in the gas phase at atmospheric pressure for 250-350°C, while Huang and Kang (1995) studied the liquid phase backward reaction at 17.2-86.2 bar and 200-260°C (Huang & Kang, 1995; Wang et al., 2008). Therefore, reaction kinetics were written separately for the forward reaction and backward reaction.

Table 3.2. Method for physical property calculation.

Physical property	Method
Forward reaction	
Pure component	
Heat capacity	DIPPR (with parameters from Aspen Properties) (Aly & Lee, 1981)
Thermal conductivity	DIPPR (with parameters from Aspen Properties) (R.C Reid et al., 1987)
Vapour viscosity	DIPPR (with parameters from Aspen Properties) (R.C Reid et al., 1987)
Enthalpy	Integration of DIPPR with heat of formation (with parameters from Aspen Properties) (Aly & Lee, 1981)
Mixture	
Thermal conductivity	Wassiljewa-Mason- Saxena equation (R.C Reid et al., 1987)
Vapour viscosity	Wilke & Herning with Zipperer approximation (R.C Reid et al., 1987)
Backward reaction	
Pure component	
Heat capacity	Reduced model of Peng-Robinson equation of state
Thermal conductivity	DIPPR (with parameters from Aspen Properties) (R.C Reid et al., 1987)
Liquid viscosity	DIPPR (with parameters from Aspen Properties) (R.C

	Reid et al., 1987)
Liquid phase enthalpy	Reduced model of Peng-Robinson equation of state
Gas phase enthalpy	Integration of DIPPR with heat of formation (with parameters from Aspen Properties) (Aly & Lee, 1981)
Mixture	
Thermal conductivity	Li mixing rule with Rackett liquid volume (Rackett, 1970; R.C Reid et al., 1987)
Liquid viscosity	Andrade liquid mixture viscosity (R.C Reid et al., 1987)

Referring to case I-2 in the work of Wang et al. (2008), the reaction rates for the forward reaction can be formulated as (Wang et al., 2008):

$$r_1 = k_{sr1} K_{TDC} P_{TDC} / \Delta^7, \quad (1)$$

$$r_2 = k_{sr2} K_{CDC} P_{CDC} / \Delta^7, \quad (2)$$

$$r_3 = k_{sr3} K_{TT} P_{TT} / \Delta^5, \quad (3)$$

$$r_4 = k_{sr4} K'_{CDC} P_{CDC} / \Omega, \quad (4)$$

$$r'_1 = k'_{sr1} K_{TT} K_{H_2} P_{TT} P_{H_2}^3 / \Delta^7, \quad (5)$$

$$r'_2 = k'_{sr2} K_{TT} K_{H_2} P_{TT} P_{H_2}^3 / \Delta^7, \quad (6)$$

$$r'_3 = k'_{sr3} K_{NP} K_{H_2} P_{NP} P_{H_2}^2 / \Delta^5, \quad (7)$$

$$r_4' = k_{sr4}' K_{TDC}' P_{TDC} / \Omega, \quad (8)$$

where $\Delta = 1 + K_{CDC}P_{CDC} + K_{TDC}P_{TDC} + K_{TT}P_{TT} + (K_{H_2}P_{H_2})^{1/2} + K_{NP}P_{NP}$, and

$$\Omega = 1 + K_{TDC}' P_{TDC} + K_{CDC}' P_{CDC}$$

The rate coefficient is given by:

$$k_{si} = A_{si} exp(-E_i/RT), \quad (9)$$

And the adsorption constant is given by:

$$K_i = A_i exp(-\Delta H_i/RT). \quad (10)$$

For the above equations, r_i and r_i' represent reaction rates as shown in Scheme 1.1. P_i is the partial pressure. A_{si} and A_i denote frequency factors. E_i and ΔH_i are activation energy and heat of reaction, respectively. The above parameters were reproduced from the Arrhenius plot of rate coefficients and Van't Hoff plot of adsorption coefficients in their work (Wang et al., 2008). Note that reversed reaction rates (represented as r_i') should also be included in the forward reaction since it is reversible.

The axial mass balances for the forward reaction are then formulated as (Wang et al., 2008):

$$\frac{dF_{TDC}}{dW} = -r_1 + r_1' + r_4 - r_4', \quad (11)$$

$$\frac{dF_{CDC}}{dW} = -r_2 + r_2' - r_4 + r_4', \quad (12)$$

$$\frac{dF_{TT}}{dW} = r_1 - r_1' + r_2 - r_2' - r_3 + r_3', \quad (13)$$

$$\frac{dF_{NP}}{dW} = r_3 - r_3', \quad (14)$$

$$\frac{dF_{H_2}}{dW} = 3(r_1 - r_1' + r_2 - r_2') + 2(r_3 - r_3'), \quad (15)$$

where F_i represents flow rate and Wrepresents the weight of catalyst which can be related to position along the axial direction of the reactor.

Adapted from Huang and Kang (1995), the mass balances for the backward reaction are given as (Huang & Kang, 1995):

$$r_{1r}' = \frac{\eta}{\dot{V}\rho_p(1-\varepsilon)} k_{sr1r}' F_{TT}, \quad (16)$$

$$r_{2r}' = \frac{\eta}{\dot{V}\rho_p(1-\varepsilon)} k_{sr2r}' F_{TT}, \quad (17)$$

$$r_{3r}' = \frac{\eta}{\dot{V}\rho_p(1-\varepsilon)} k_{sr3r}' F_{NP}, \quad (18)$$

$$r_{4r} = \frac{\eta}{\dot{V}\rho_p(1-\varepsilon)} k_{sr4r} F_{CDC}, \quad (19)$$

$$\frac{dF_{TDC}}{dW} = r_{1r}' + r_{4r}, \quad (20)$$

$$\frac{dF_{CDC}}{dW} = r_{2r}' - r_{4r}, \quad (21)$$

$$\frac{dF_{TT}}{dW} = -r_{1r}' - r_{2r}' + r_{3r}', \quad (22)$$

$$\frac{dF_{NP}}{dW} = -r_{3r}', \quad (23)$$

$$\frac{dF_{H_2}}{dW} = -2r'_{3r} - 3r'_{1r} - 3r'_{2r}, \quad (24)$$

where r_{ir} and r'_{ir} are the reaction rates corresponding to Scheme 1, the "r" at the end is used to distinguish from the forward reaction. η is a correction factor, which was assumed to be 0.8 and is explained in the next section. $\dot{V}$ is the volumetric flow rate of the mixture. ρ_p is the density of catalyst, which was assumed to be 3.66 g/cm^3 as the density of γ-Al_2O_3 (Alvarez et al., 1995). ε is the bed porosity, which is given by (Adams & Barton, 2009):

$$\varepsilon = 0.38 + 0.073\left(1 - \left(\frac{D_{shell}}{D_p - 2}\right)^2 \Big/ \left(\frac{D_{shell}}{D_p}\right)^2\right), \quad (25)$$

where D_{shell} and D_p represent the shell diameter and catalyst particle diameter, respectively. D_p was assumed to be 0.016 m (Ghouse & Adams, 2013).

Unlike the mass balances, the momentum and energy balances are the same for forward and backward reactions.

Adapted from the Ergun equation, the momentum balance is formulated as (Ergun & Orning, 1949):

$$\frac{dP}{dW} = -\frac{v}{D_p}\frac{(1-\varepsilon)}{\varepsilon^3}\left(150(1-\varepsilon)\frac{\mu}{D_p} + 1.75\rho v\right)\left(\frac{1}{A_{cs}(1-\varepsilon)\rho_p}\right), \quad (26)$$

where v, μ, and ρ are the superficial velocity, viscosity, and density of the mixture. A_{cs} is the cross-sectional area of the geometry through which the mixture flows (cross-sectional area of shell subtracting cross-sectional area of tubes).

The energy balances are formulated as Equation (27) and (28), in a form of explicit expression for the shell and tube side temperatures (Incropera et al., 2011; Smith, 1981). Although heat capacity is a function of temperature, the rate of change of heat capacities of the gases with respect to the change in catalyst weight is small. Therefore, heat capacity is assumed to be constant for a given integration step, although the value of the constant heat capacity used is recalculated every integration step using updated values of temperature.

$$\frac{dT_{shell}}{dW} = \frac{1}{\sum_{i=1}^{n} F_i C_{pi}} \left(U \Delta T \frac{dA}{dW} - \sum_{j=1}^{m} r_j \sum_{i=1}^{n} \beta_{j,i} H_i \right) \tag{27}$$

$$\frac{dT_{tube}}{dW} = \frac{1}{C_{pH_2O} \dot{M}_{H_2O}} U \Delta T \frac{dA}{dW} \tag{28}$$

where

$$U \frac{dA}{dW} = 1 \Bigg/ \left(\frac{1}{h_f \pi D_{tube,outer} N_{tube} \frac{dL}{dW}} + \frac{ln\left({D_{tube,outer}}/{D_{tube,inner}} \right)}{2\pi k_w \frac{dL}{dW}} + \frac{1}{h_{H_2O} \pi D_{tube,inner} N_{tube} \frac{dL}{dW}} \right) \tag{29}$$

C_p is molar heat capacity and C_{pH_2O} is the steam/water heat capacity on mass basis, at the current temperature. H_i is the enthalpy of each component at the current temperature, which is calculated according to Table 3.2. They are temperature-dependent, and were estimated at the current temperature in every iteration step. ΔT is the temperature difference between the shell side and the tube side. $\beta_{j,i}$ represents the stoichiometry of species i in reaction j. $\dot{M}_{H_2O}$ denotes

the mass flow rate of steam/water, which is constant for a given hour of application. k_w is the thermal conductivity of the tube wall, and was assumed to be 69.23 W/(m·K) as steel (Harper, 2006). Note that equation (28) equals zero for stage 2 since the tube side temperature stays at the boiling temperature at the current pressure, by assuming that the pressure drop was small enough so that the boiling point did not change. In equation (29), the three terms in the denominator are convection through the shell side to the tubes, conduction through the tubes, and convection through the tube side to the tubes, respectively. The heat transfer coefficients are estimated as (Babu & Rao, 2007; Coulson & Richardson, 1979; Smith, 1981; Wakao, 1982):

$$h_{f,forward} = \frac{k_f}{D_p}(0.203Re^{0.33}Pr^{0.33} + 0.22Re^{0.8}Pr^{0.4}) \quad (30)$$

$$h_{f,backward} = \alpha\frac{k_v}{D_p}(0.203Re_v^{0.33}Pr_v^{0.33} + 0.22Re_v^{0.8}Pr_v^{0.4}) + (1-\alpha)\frac{k_l}{D_p}0.6Re_l^{0.47}Pr_l^{0.33} \quad (31)$$

$$h_{H_2O} = \frac{k_{H_2O}}{D_{tube,inner}}0.023Re_{H_2O}^{0.8}Pr_{H_2O}^{0.3} \quad (32)$$

Where the Reynolds number $\mathrm{Re} = \rho v D/\mu$ and the Prandtl number $\mathrm{Pr} = \mu C_p/k$. The physical properties equations in Table 3.2 were used in the computation of Re and Pr such that they account for the flow mixture and change across the axial position of the reactor. The diameter in the expression of Reynolds number should be the catalyst particle diameter for the shell side, and the tube inner

diameter for the tube side. In equation (31), α is the volume averaged void fraction or called gas hold up. It is defined as the volumetric flow rate of gas divided by the sum of volumetric flow rate of both gas and liquid. It was also used to estimate physical properties of the two-phase mixture. In equation (31), α was used to joint correlations for gas phase and liquid phase (Brennen, 2005). A single heat transfer correlation for two-phase flow in such geometry has not yet been studied to our knowledge.

The forward and backward reaction models were developed in MATLAB 2016b, and ode23s functions were used for the ODEs in the models. The known boundary conditions of the ODEs are the known conditions (flow rates, temperatures, pressures, compositions) of the tube and shell inlet streams (as resulting from Aspen Plus simulations). However, because the reactor uses counter-current flow, this does not result in an initial value problem that can be integrated directly with an ODE solver in MATLAB. Moreover, the total reactor weight W is not known *a priori.* Instead, an initial value problem was formulated by defining W=0 to be the shell inlet, with known boundary conditions on the shell side defined at W=0, such as $T_{shell}|_{W=0}$, and $P_{shell}|_{W=0}$. The tube side boundary conditions at W=0 (the tube outlet), such as $T_{tube}|_{W=0}$, and $P_{tube}|_{W=0}$, which are unknown, were guessed, resulting in a solvable initial value problem. The simulation was then integrated from W=0 to $W=W_{max}$ (where the reaction achieved 95% conversion), and the resulting computed tube side variables at $W=W_{max}$ were compared against the known values (the tube inlet conditions). If

the difference was greater than some small tolerance, new guesses were generated for the tube side variables at W=0 and the procedure was repeated iteratively until convergence was achieved. Note that with this approach, the forward reaction starts from stage 1 to 3 with W=0 at the start of stage 1, but the backward reaction starts from stage 3 to 1 with W=0 at the start of stage 3.

Because the model equations are different in each stage, and the length of each stage (in terms of W) is not known *a priori*, the integration algorithm included checks to detect a stage change (for example, when the tube temperature drops below the boiling point). The step occurring after the detected event was rejected and the previous time-step results were used to re-initialize the problem starting at the beginning of the new stage. Because the integration step sizes were small, advanced techniques to adjust integration step-sizes to find the event location with high precision were not used.

For the backward reaction, the rate of heat release from the exothermic reaction is far faster than the rate of heat transfer to the tube side. This makes heat management an important consideration in the design of the reactor. For example, feeding all of the reactants (mainly NP and H_2) together at the shell inlet results in unreasonably large temperatures in the shell side near the entrance. To solve this problem, the proposed design feeds all of the H_2 without NP at the shell inlet. There are many NP injection points into the shell down the length of the reactor in which a small amount of NP at its storage temperature (82°C) and pressure of the reaction are injected. The injection locations were determined

during ODE integration by event detection in a similar manner to detecting the onset of a new stage: whenever the shell temperature dropped below 400°C, between 0.5 and 2 kmol/hr (which varied along the length of the reactor) of NP was injected at the current W, which typically resulted in a local temperature increase to approximately 1 - 5°C (also varied along the length of the reactor). The NP injections were treated as an input to the next ODE integration, therefore no change was made to the mass balances while the enthalpy term of the injection was added to the energy balances. The actual amount to inject at each point was determined manually through a trial-and-error process. The correction factor η is used to account for this change as the reaction might be slower due to additional mixing when NP is injected.

3.2.3. Phase 3: Integration of base-case models

To integrate the base-case Aspen Plus models with the reactor models, the sequence steps shown in Figure 3.4 were followed (the upper part). PSO was implemented on the forward reaction mode to minimize the reactor weight with a constraint that the reaction conversion achieved 95%. The optimization problem was formulated as follows:

$$min\ \rho_{steel}\pi L\left(\left(D_{shell,outer}/2\right)^2-\left(D_{shell,inner}/2\right)^2+N_{\mathrm{tube}}\left(\left(D_{\mathrm{tube},outer}/2\right)^2\right)\right.$$
$$\left.-\left(D_{tube,inner}/2\right)^2\right)$$

$$s.t.\ \left(F_{TDC}|_{W=0} - F_{TDC}|_{W=W_{max}}\right)/F_{TDC}|_{W=0} \geq 0.95,$$

where the density of the steel ρ_{steel} was assumed to be 7.8 g/cm^3 (Perry & Green, 2008). L is the reactor length. The decision variables included shell inner diameter, tube outer diameter, the tube-sheet layouts (square pitch or triangular pitch), and the reactor length. The reactor length (or equivalently, the catalyst weight) was allowed to be as long as necessary for the reaction to achieve 95% conversion. Peters and Timmerhaus (1991) summarize different conventional combinations of shell inner diameters, tube outer diameters, and tube-sheet layouts; and the maximum number of tubes for each combination (Peters & Timmerhaus, 1991). The shell outer diameter and tube inner diameter were calculated by assuming that the wall thickness was 1/20 of the inner diameter (Tooley & Dingle, 2013).

Since the optimization problem was formulated to include various shell-and-tube configurations, a number of infeasible points were expected such as too large pressure drop that caused the reaction to terminate. Hence, PSO was a suitable optimization tool for this problem as it could identify feasible points when it searched the whole space and found very good options among the feasible points. Again, it did not guarantee a global optimum, but only good feasible results were needed.

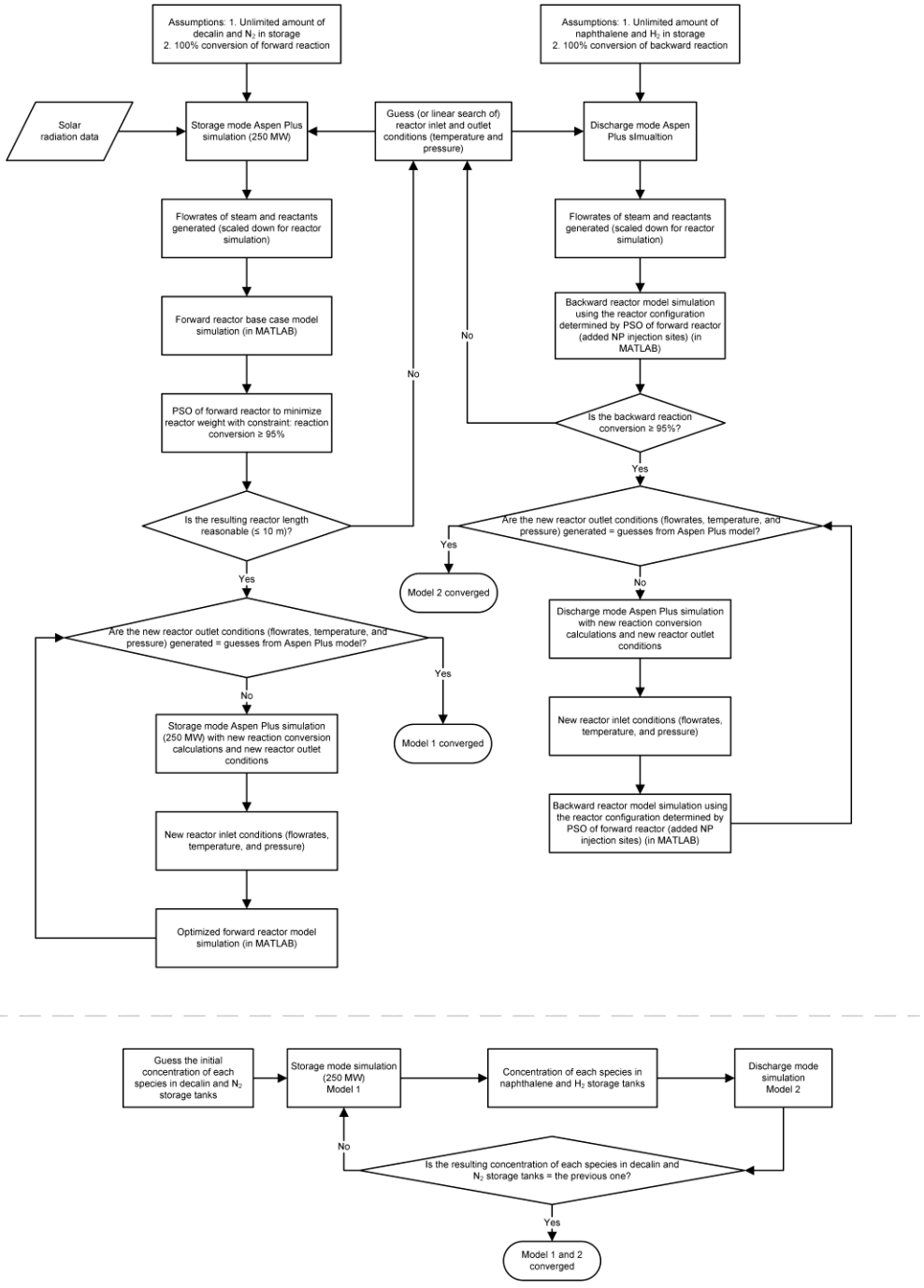

Figure 3.4. The simulation sequence for integrating the base-case models. The upper part is the sequence for integrating base-case Aspen Plus models with the reactor models. The lower part is the sequence for integrating the storage and discharge mode models.

By following the sequence in the upper part of Figure 3.4, the models converged when the shell inlet was 1.17 bar and 265°C for the forward reaction mode and 51.7 bar and 400°C for the backward reaction mode. However, the compressor power consumption predicted by the integrated model was very high (37% of the net power production) due to the pressure increase from 1 to 8.5 bar (for the membrane operation) and from 0.2 to 52 bar (for H_2 storage). To reduce the power usage for this part, the shell inlet pressure for the forward and backward reaction modes were changed to 2.12 bar and 34.5 bar respectively, while keeping the temperature settings unchanged. By reducing this pressure difference, the power consumption of the compressors was reduced to 30% of the net power production. However, a longer reactor is required to achieve the target reaction conversions. Hence, the maximum reactor length constraint on Figure 3.4 was changed to 20 m for model convergence. In addition, it was assumed that the forward reaction kinetics are still applicable at 2 bar, even though they were only developed at about 1 bar (Wang et al., 2008). Similarly, the relationship between rate constants and temperature of the backward reaction for 34.5 bar were assumed to be the same as that for 51.7 bar, based on the linearity of the Arrhenius plot in Huang and Kang (1995). Also, linear extrapolation of rate constants was assumed for temperatures out of the range of the study (Huang & Kang, 1995).

By integrating the storage mode Aspen Plus model with the MATLAB forward reaction model, and the discharge mode model with the backward reaction model;

two integrated models were obtained: Model 1 and Model 2. However, in order to converge the model equations which relate to chemical compositions of the storage tanks, the Aspen Plus and MATLAB portions of the models had to be solved iteratively. The sequence shown in the bottom of Figure 3.4 was followed to integrate the storage and discharge mode models (Model 1 and Model 2) to ensure the chemical compositions in each tank in the two models converged. Model 3 (storage mode with second base-load: 120 MW) was then obtained by changing the gross power production setting of Model 1 from 250 MW to 120 MW. Model 4 (transient mode with base-load: 120 MW) was the combination of Model 2 and the solar-steam cycle part of Model 1. Note that these models are representative of only one reactor, although the actual design uses many identical reactors. For example, Model 3 requires around 49 reactors (treated as continuous variables in Phase 3 and corrected in Phase 4) in parallel operating in backward reaction mode to achieve the base-load power production.

3.2.4. Phase 4: Overall System Simulations

A simulation strategy algorithm was developed in Microsoft Excel VBA (Visual Basic for Applications) by following the sequence shown in Figure 3.5. The Excel Aspen Simulation Workbook was used as an interface to connect the VBA algorithm with the base case models (Model 1 to 4). As shown in Figure 3.5, the hourly solar radiation data (from July 1st 8:00 am, 2011 to July 1st 7:00 am, 2012)

were taken as inputs to the VBA algorithm for Round 1 simulations. For each solar radiation data point, the algorithm chose an appropriate model among Model 1 to 4, based on the current solar radiation and chemical storage. These steady-state base case models were set to produce power on base-loads of either 250 MW or 120 MW if possible, and they could also produce power below the base-loads depending on the current available solar radiation and chemical storage. As outputs to the VBA, each case model returned the number of reactors used (as a continuous variable) and the key parameters such as steam flowrate in the solar-steam cycle, steam flowrate and reactant flowrates to the reactor. By following the algorithm, 8784 steady-state simulations were run case-by-case according to the hourly solar radiation data in Round 1. However, it was not practical to have a non-integer number of reactors. Hence, Round 2 simulations were run by taking the rounded numbers of reactors and the key parameters from Round 1 as input data. In Round 2, each case from Round 1 was re-run with the new input data. The chemicals storage availability was also updated between each case simulation since the simulation results were different than those in Round 1. The resulting electricity production of each case was also different than that in Round 1. For example, a case that produced base-load of 250 MW in Round 1 would result in producing slightly more or less than the base-load in Round 2.

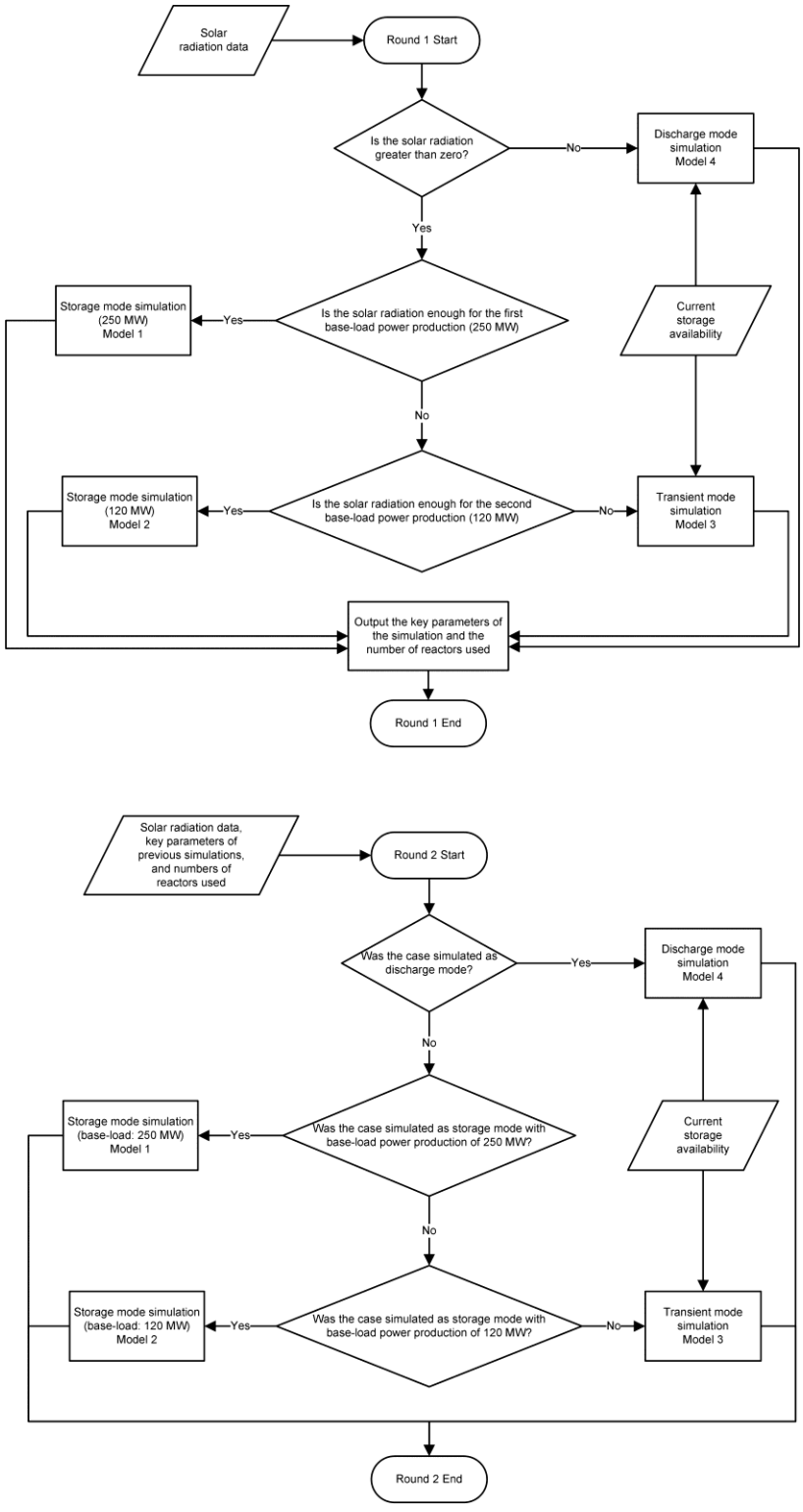

Figure 3.5. The VBA sequence for the overall system simulations.

4. Results and Discussion

4.1. Reactor Results

The final reactor configuration chosen is shown in Figure 4.1. The shell was designed to be packed with catalyst particles and 137 tubes arranged in a square pitch. It was determined through simulation studies that 67 injection sites are required, which are located along the reactor length (9.37 m long) on the shell wall with an average distance of 0.14 m in between each site. These injection sites were used only for the backward reaction. The forward reaction needed a longer reactor to complete the reaction with satisfied conversion, which was determined to be 18.74 m in length (double the length of the designed reactor). In practice, the forward reaction would require two reactors in series (connecting two designed reactors head-to-tail) in operation as shown in Figure 4.1.

The simulation results showed that the worst-case number of the '9.37m' reactors was 282 (during storage mode from 1 pm to 2 pm on March 2, 2012) if the system were designed to capture all available excessive solar energy while providing base-load power production within that hour. The total footprint of 282 reactors is around 0.1 hectare, which is 1/20 of the footprint of the solar field. In practice, one would likely construct the system with much fewer reactors and simply not recover all available solar energy during the most intense times of the year. For example, by constructing only 180 reactors, one could still recover 92%

of all available excessive solar energy in the year. Determining the optimal number of reactors with this trade-off in mind is not trivial and out of the scope of this work, which would require a complete economic analysis under the uncertainty of solar intensity variations, market prices, electricity demand, and other factors.

The discharge mode and transient mode required less than 50 of the '9.37m' reactors in the worst case. The forward reaction (storage mode) requires much more reactors than the backward reaction (discharge or transient mode) because the forward reaction needs a large amount of N_2 as a sweep gas to maintain the desired conversion. As future work, further kinetic studies on the reaction at different pressures, temperatures, and sweep gases might help to identify better reaction conditions to use based on the system as a whole.

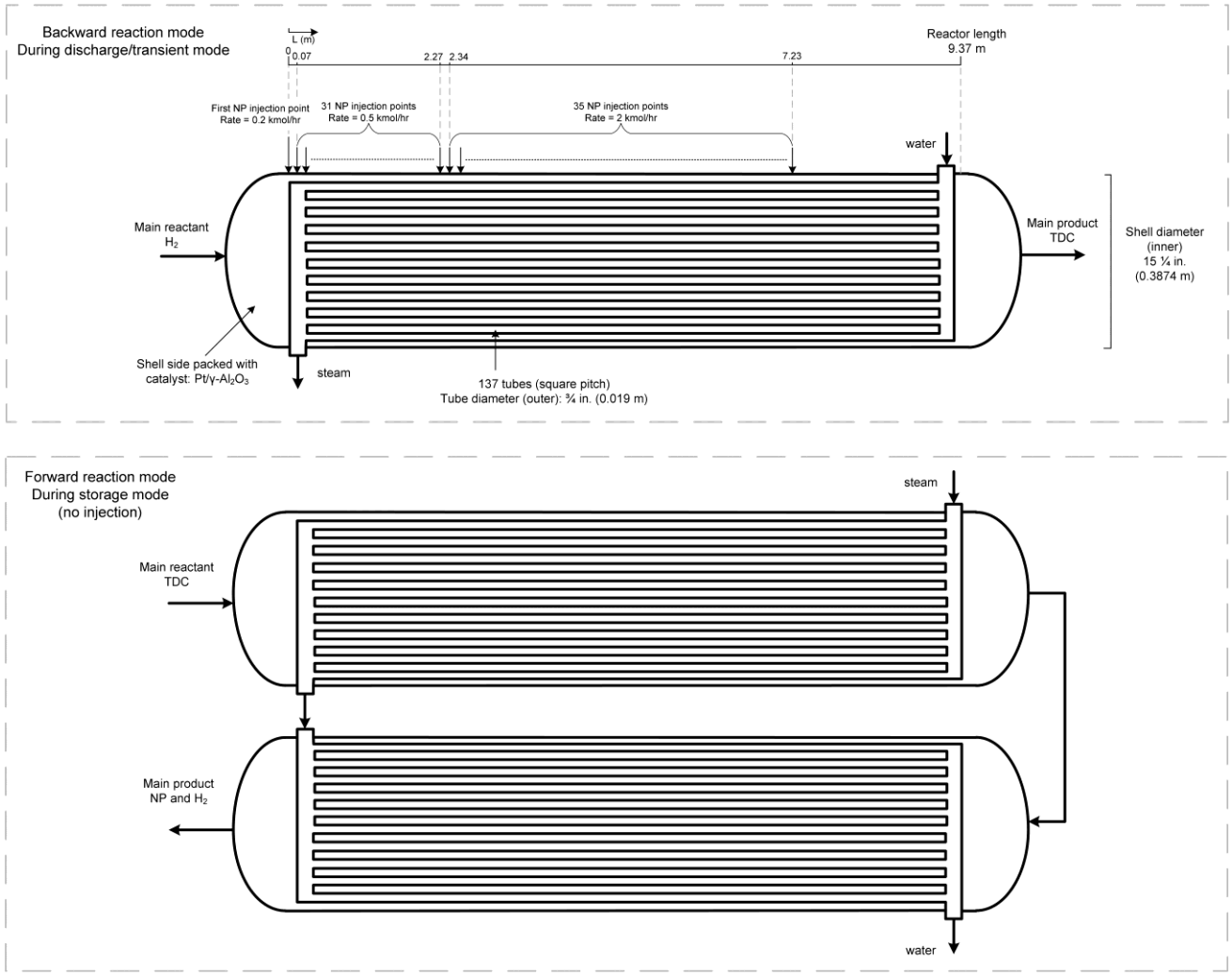

Figure 4.1. Reactor configuration specifications.

Figure 4.2 shows the temperature profiles and the flowrate profiles of both the forward reaction and backward reaction in a single reactor (or two-reactor-in-series for the forward reaction). The arrows on the temperature profiles represent the direction of the flows. For the forward reaction, reactants (mostly TDC as the major product of the backward reaction, N_2 as sweep gas which is not shown in the figure, and trace other species) enter through shell side at 265°C and pass through stage 1 to 3, absorbing heat from the tube side and forming NP and H_2. The products leave the reactor at 361.5°C with 100% conversion of both TDC and CDC. The selectivity to NP and TT were found to be 99.88% and 0.12%, respectively. In the counter-current direction, steam at 550°C enters stage 3 of the reactor on the tube side; and releases heat until its dew point (303.38°C at 90 bar) is reached, where stage 2 begins (Haar, 1984). The temperature stays constant for the phase-change stage and drops to 301°C at the other end of the reacto

While running the backward reaction, H_2 with a small amount of N_2 (left from the membrane separation) enters stage 3 on the shell side at 400°C, which is the opposite direction of the forward reaction (still shown from left to right on the figure). NP with trance TT is then injected through the injection sites. As can be seen in the figure, each step change on the NP flowrate profile represents an injection. For a better illustration of the flowrate profiles of NP, CDC, and TT, Figure 4.2 shows flowrate profiles without H_2 and TDC as well as a magnified window of stage 3. The specifications of injection can be seen in Figure 4.1. The

injections successfully keep the reaction temperature around 400°C for most of the time, so that the backward reaction completed with 100% conversion of NP. The selectivity to TDC, CDC, and TT was computed to be 97%, 2%, and 1%, respectively.

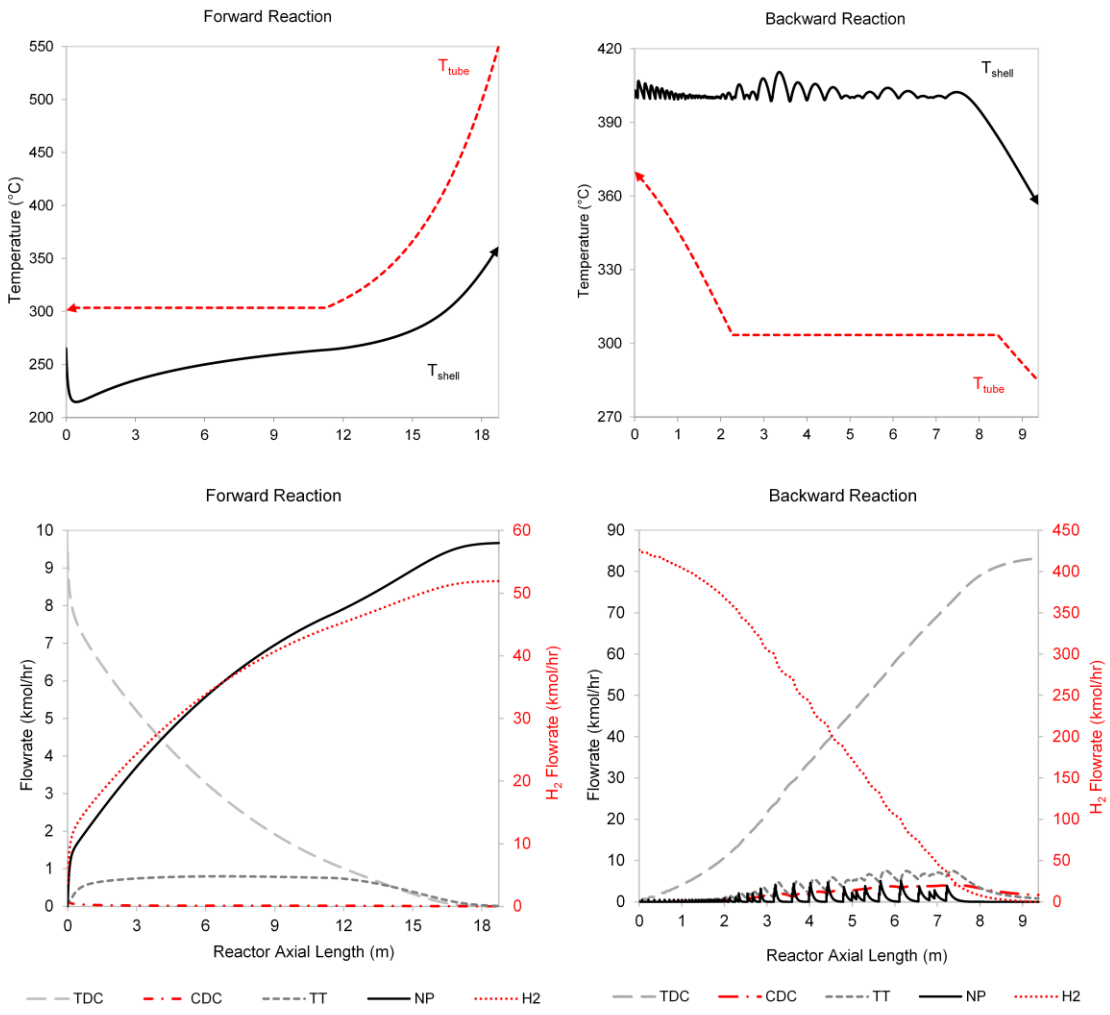

Figure 4.2. Axial profiles of temperature and reactant flowrates during the forward and backward reaction.

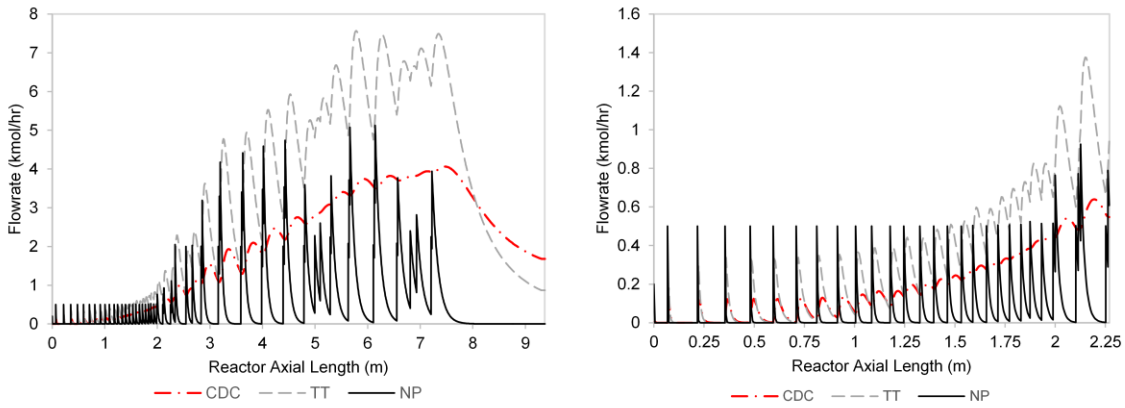

Figure 4.3. Axial profiles of reactant flowrates during the backward reaction (only showing cis-decalin, tetralin, and naphthalene) and a magnified window of stage 3.

4.2. Overall System Results

The results of the overall system simulations showed that the predicted total annual production from July 1st, 2011 to July 1st, 2012 was 861 GWh. The overall plant efficiency was found to be 14.6%, which is defined as the total gross power production over the total available solar energy in the year. Comparable to the existing CSP plant, Solana Generating Station, the projected production of the Solana plant was 944 GWh and the actual production from 2014, 2015, and 2016 was 604 GWh, 719 GWh, and 644 GWh, respectively (NREL, 2015c; U.S. Department of Energy, 2017a). The monthly production profile predicted by the model is shown in Figure 4.4. The system produced much more power in summer than winter as expected. To illustrate the electricity production on daily basis, Figure 4.5 shows the daily model predicted production for the month of

March, 2012. It can be seen that the power production varied according to the weather conditions.

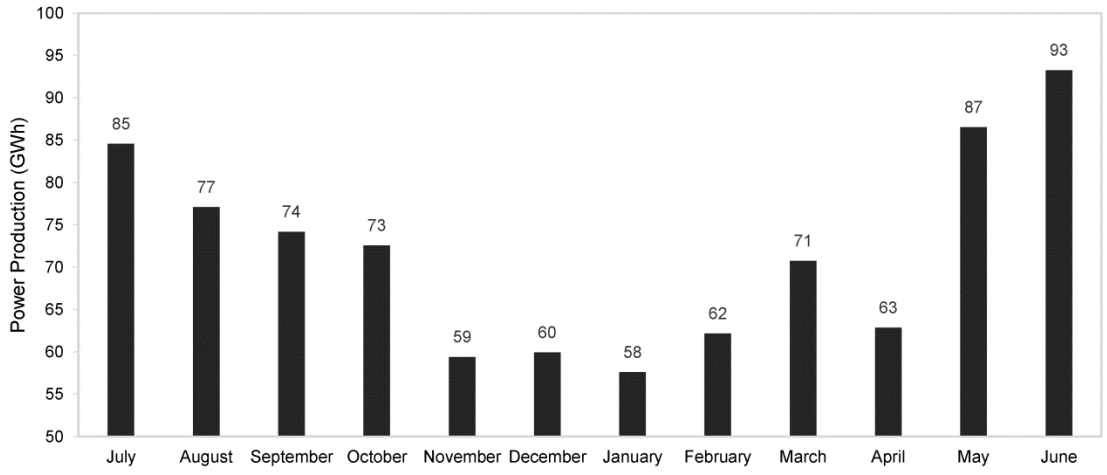

Figure 4.4. Model predicted monthly electricity production.

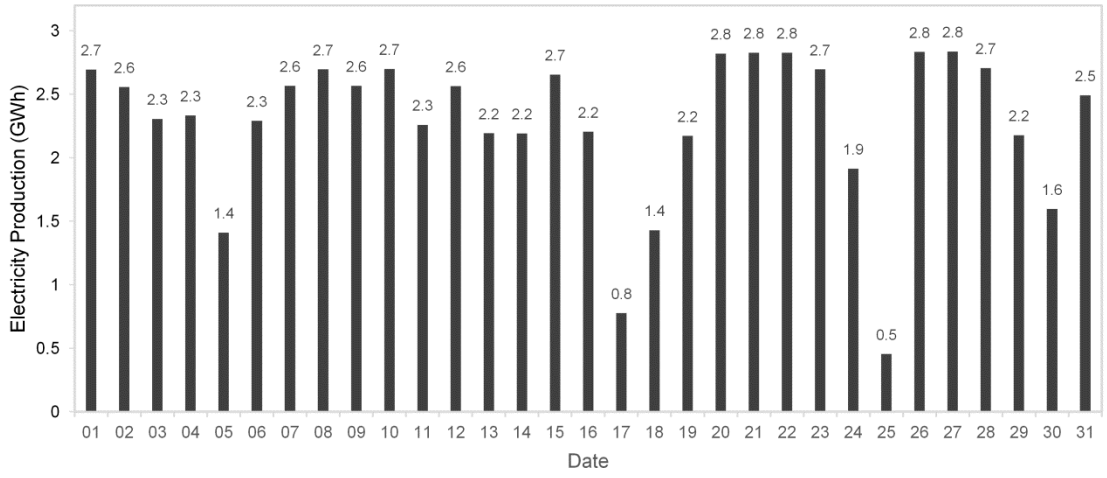

Figure 4.5. Model predicted daily electricity production in March, 2012.

Figure 4.6 shows the model predicted hourly electricity production profile (the bottom figure) on a typical summer day, July 8th, 2011. At 6 am, the plant produced as much power as the sunlight could supply (below 120 MW). In the next hour, the available solar energy was enough for the second base-load production (120 MW) and the excessive solar energy was stored through the thermochemical storage system. From 8 am, the system produced power at 250 MW and stored the extra solar energy until 6 pm. The transient mode was switched on at 7 pm. Energy was discharged from the storage system to compensate the insufficient sunlight during this hour, to produce power at 120 MW. The discharge mode took over at 8 pm as the sunlight diminished, lasting for two hours until the stored energy was depleted.

For illustrative purposes, Figure 4.6 includes an example power demand curve that was taken and scaled from historical grid data for Ontario, Canada (IESO, 2016) (since power demand curves for the area served by the Solana station were unavailable to our knowledge). This figure highlights the mismatch between the peaks of sunlight and power demand, showing that the proposed CSP plant could still produce power in the evening (without adequate sunlight) while the power demand is still high. Although power demand curves were not considered in this work, designing and simulating the CSP plant for peaking power demand might be considered in future work.

Accordingly, the volume profiles of the main species TDC and H_2 in the storage tanks on July 8th, 2017 can be seen as the upper part of Figure 4.6. The TDC

volume continuously decreased as the energy was being stored through the forward reaction until 6 pm. It started to fill up at 6 pm since TDC was produced by the backward reaction during the transient or discharge mode. The H_2 volume, on the contrary, increased and then decreased in accordance with the energy storing and discharging in the storage system. Note that the TDC volume did not recover to its original level in a daily cycle. The root cause was the incomplete membrane separation when separating H_2 from N_2 (separating around 78% of H_2). H_2 became the limiting reactant for the backward reaction. NP was left over from the reaction since it was in excess, which caused the incomplete recovery of TDC. In a result, the system kept consuming TDC and building up NP.

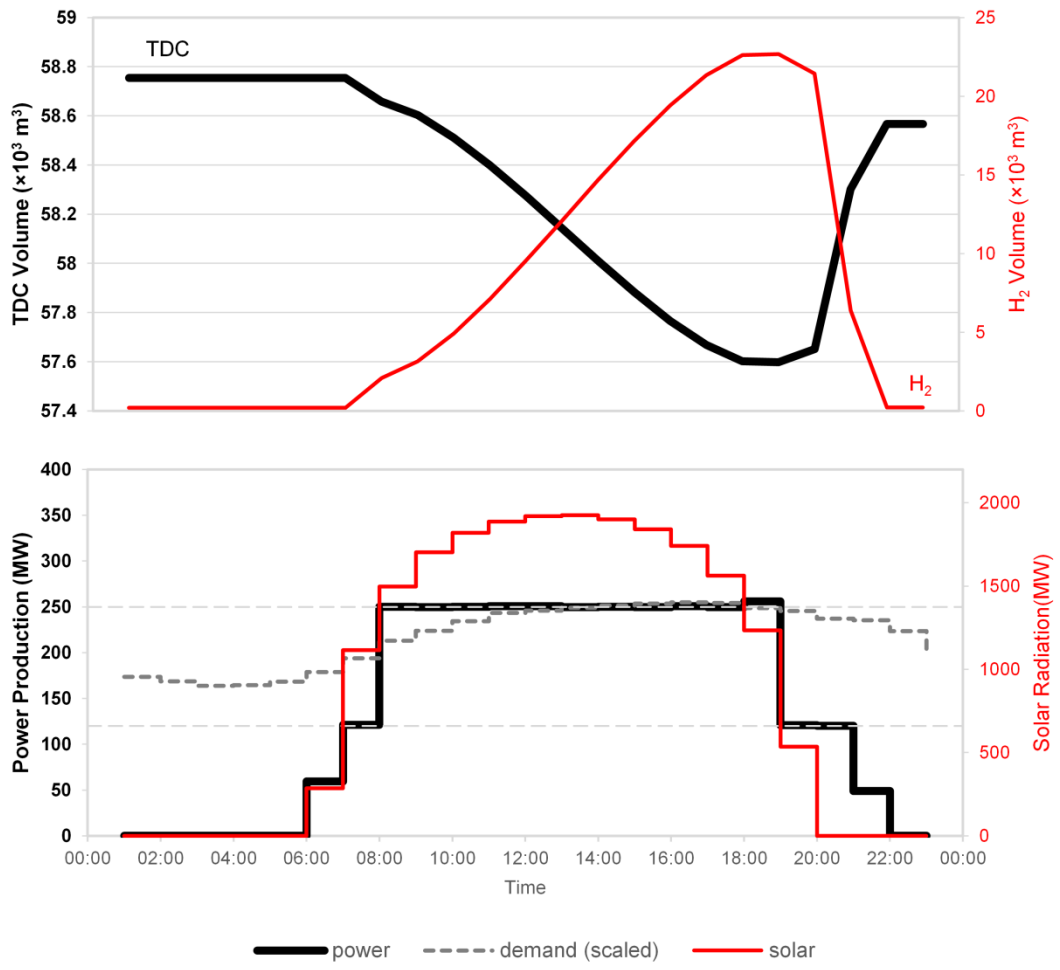

Figure 4.6. Model predicted electricity production profile and storage volume profiles of chemicals on July 8th, 2011. On the bottom figure, power production and demand curves are read from the primary axis on the left, and solar radiation is read from the secondary axis on the right.

Figure 4.7 shows the simulation results for a cloudy day in winter. Unlike the profiles on July 8th, the profiles on January 29th have more up-and-down zigzag shapes. The CSP plant was switched between the storage mode and the transient mode with the two base-load power production settings according to the

intermittent sunlight. From the storage volume profiles, it can be easily seen that the CSP plant was operating in transient mode from 11 am to 12 pm, as the TDC storage increased and H_2 storage decreased. The CSP plant was capable of extending the production hours to 1-2 hours after the sunlight disappeared. This is low compared to Solana Generating Station which claims a 6 hour storage capacity with the molten salt storage system (NREL, 2015c), although based on their actual reported production, the actual average daily energy stored is more likely in the 2-3 hour range. In addition, the low storage capacity of the decalin-based system is largely explained by the low discharge efficiency, which produces only 18.8 MWh of electricity per 100 MWh of chemical energy stored (based on heats of formation). The large parasitic load of the compressors is a major factor in this low efficiency, which could be improved by changing the operating pressures of the forward and backwards reaction. However, this could not be explored in this study because no kinetic information on the forward and backward reaction at other pressures is available.

As mentioned above, the system slowly decays over cycles as NP builds up. If designing the system for one year's worth of cycles, the sizes of decalin, naphthalene, H_2, and N_2 storage tanks (as shown in Figure 3.1) were found to be 6×10^4 m^3, 3.8×10^4 m^3, 4×10^4 m^3, and 3×10^5 m^3, respectively. However, one could consider using fresh H_2 to convert the excessive NP back into TDC and CDC via the backward reactors at the end of each day. In this case, the storage sizes of

decalin and naphthalene could be reduced to 1.7×10^3 m^3 and 1.4×10^3 m^3, respectively.

Compared to the existing CSP plant the Solana Generating Station, the proposed thermochemical storage system was relatively larger, but safer since chemicals were stored at much lower temperature. It was reported that Solana holds 125,000 metric tons of molten salt, which is around 5.7×10^4 m^3 in volume. It requires smaller space than the thermochemical storage system, but the molten salt has to be stored at up to 390°C (Peltier & PE, 2014). For the proposed thermochemical storage system, naphthalene would be stored at 82°C and the other chemicals could be stored at room temperature or ambient temperature.

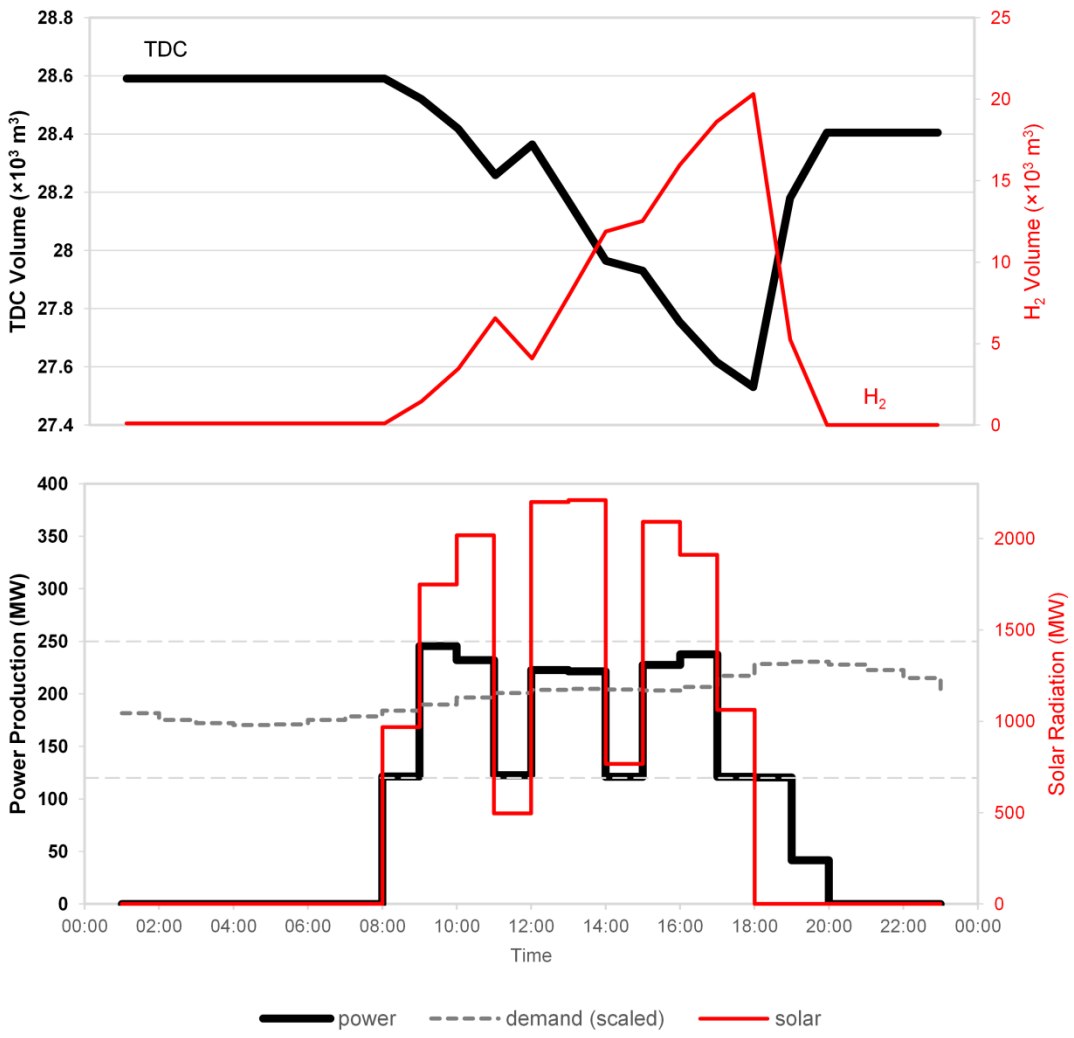

Figure 4.7. Model predicted electricity production profile and storage volume profiles of chemicals on January 29th, 2012. On the bottom figure, power production and demand curves are read from the primary axis on the left, and solar radiation is read from the secondary axis on the right.

5. Conclusions and Future work

In this work, the feasibility and effectiveness of an integrated DSG CSP plant with a decalin/naphthalene thermochemical storage system was investigated through simulations for 8784 cases in accordance with historical hourly solar radiation data over a year. It was found that the integrated plant was able to extend base-load power production for 1 to 2 hours when sunlight completely disappeared on a single day. The plant was proven to be feasible as it continuously stored and discharged energy to maintain the base-load power production with high conversion and reversibility of decalin/naphthalene reactions. However, it was found that the whole system was not completely reversible due to incomplete membrane separation of H_2 from N_2, meaning that the storage capabilities of the chemicals decayed over time. Thus, the system requires periodic recharging of the storage chemicals. Compared to the molten salt storage system, the proposed decalin/naphthalene thermochemical storage system has lower storage temperature (at ambient temperature except for naphthalene which is stored at 82°C). If the gradual storage capacity degradation issue could be remedied, the required storage size would be smaller than the molten salt storage system. As an overall recommendation, the proposed integrated DSG CSP plant with a decalin/naphthalene thermochemical storage system could be a strong alternative to CSP plants with molten salt storage systems.

Since this work is the first known investigation of a DSG CSP plant with a decalin/naphthalene thermochemical storage system to the best of our knowledge, several assumptions were made during model simulations for this conceptual design, such as limiting possible reaction pressures to ranges in which the kinetics were known, instead of where they might be more optimal from a systems perspective. Therefore, additional experimental studies on the reaction kinetics in the pressure range of 2 - 35 bar would be very beneficial. This brings to the first potential research study for future work shown as follows:

Future work 1: Experimental reaction kinetics studies on the decalin/naphthalene reactions in the pressure range of 2 – 35 bar and temperature range of 200 – 450 °C. These experimental reaction kinetics under the above conditions are not found in the literature but essential for the applications on thermochemical storage system. By rough calculations on forward reaction at 2 bar and backward reaction at 20 bar, the parasitic load of compressors could be reduced by 70% which would strongly boost the system efficiency. Moreover, if the forward reaction could take place without the N_2 sweep gas, the number of reactors needed would strongly decrease.

Future work 2: Simulations of the designed system for long term storage. This study focused only on the short term storage for maintaining a base-load power production for a few hours when sunlight diminishes, for the purpose of comparison to existing CSP plants with the molten salt storage system. However,

one of the advantages of the thermochemical storage system is long term storage as no heat loss is associated with the storage method. By reducing the base-load power output of the designed system while remaining the solar field size, the storage hour could be increase theoretically. However, a larger number of reactors and larger storage size are required. Besides, designing the system for peaking hour could also be considered.

Future work 3: Economic analysis of the designed system. Performing economic analysis would allow comparison to existing CSP plants with molten salt storage system in terms of cost-effectiveness of the system.

Other future studies include developing a flow pattern model for the steam/water two-phase flow, formally optimizing the heat integration of the plant, and analyzing alternatives to H_2/N_2 separations. These future work considerations will likely affect the competitiveness of the proposed system as an alternative to other CSP plants.

References

Abengoa Solar. (2013, April). *A New Generation of Parabolic Trough Technology*. Presented at the SunShot CSP Program Review 2013, Phoenix, AZ.

Abengoa Solar. (2014). Abengoa Solar :: Solar plants :: Third party plants :: United States. Retrieved March 10, 2017, from http://www.abengoasolar.com/web/en/plantas_solares/plantas_para_terceros/estados_unidos/

Adams, T. A., & Barton, P. I. (2009). A dynamic two-dimensional heterogeneous model for water gas shift reactors. *International Journal of Hydrogen Energy*, *34*(21), 8877–8891. https://doi.org/10.1016/j.ijhydene.2009.08.045

Air Products. (2017). PRISM® PB6050 Membrane Separators for hydrogen separation in glycol manufacturing.

Alvarez, L. J. et al. (1995). Computer Simulation of .gamma.-Al2O3 Microcrystal. *The Journal of Physical Chemistry*, *99*(51), 17872–17876. https://doi.org/10.1021/j100051a011

Aly, F. A., & Lee, L. L. (1981). Self-consistent equations for calculating the ideal gas heat capacity, enthalpy, and entropy. *Fluid Phase Equilibria*, *6*(3), 169–179. https://doi.org/10.1016/0378-3812(81)85002-9

Aristov, Y. I. et al. (1993). High-temperature chemical heat pump based on reversible catalytic reactions of cyclohexane-dehydrogenation/benzene-hydrogenation: Comparison of the potentialities of different flow diagrams. *International Journal of Energy Research*, *17*(4), 293–303. https://doi.org/10.1002/er.4440170406

Babu, B. V., & Rao, V. G. (2007). *Thermal Resistance Models for Effective Heat Transfer Parameters in Trickle Bed Reactors*.

Badie, J. M. et al. (1980). 52 Decarbonation of calcite and phosphate rock in solar chemical reactors. *Chemical Engineering Science*, *35*(1), 413–420. https://doi.org/10.1016/0009-2509(80)80114-X

Birnbaum, J. et al. (2010). A Direct Steam Generation Solar Power Plant With Integrated Thermal Storage. *Journal of Solar Energy Engineering*, *132*(3), 031014–031014. https://doi.org/10.1115/1.4001563

Bogdanović, B. et al. (1990). Active MgH2-Mg Systems for Reversible Chemical Energy Storage. *Angewandte Chemie International Edition in English*, *29*(3), 223–234. https://doi.org/10.1002/anie.199002233

Bosetti, V. et al. (2012). The future prospect of PV and CSP solar technologies: An expert elicitation survey. *Energy Policy*, *49*, 308–317. https://doi.org/10.1016/j.enpol.2012.06.024

Bowrey, R. G., & Jutsen, J. (1978). Energy storage using the reversible oxidation of barium oxide. *Solar Energy*, *21*(6), 523–525. https://doi.org/10.1016/0038-092X(78)90078-6

Brennen, C. E. (2005). *Fundamentals of Multiphase Flow*. Cambridge University Press.

Cacciola, G. et al. (1987). Chemical heat pump using heat of reversible catalytic reactions. *International Journal of Energy Research*, *11*(4), 519–529. https://doi.org/10.1002/er.4440110408

Carden, P. O. (1977). Energy corradiation using the reversible ammonia reaction. *Solar Energy*, *19*(4), 365–378. https://doi.org/10.1016/0038-092X(77)90008-1

Coulson, J. M., & Richardson, J. F. (1979). *Chemical engineering* (2nd ed. (SI units)). Oxford ; New York: Pergamon Press.

Edwards, J. H. et al. (1996). The use of solar-based CO2/CH4 reforming for reducing greenhouse gas emissions during the generation of electricity and process heat. *Energy Conversion and Management*, *37*(6), 1339–1344. https://doi.org/10.1016/0196-8904(95)00343-6

Ergun, S., & Orning, A. A. (1949). Fluid Flow through Randomly Packed Columns and Fluidized Beds. *Industrial & Engineering Chemistry*, *41*(6), 1179–1184. https://doi.org/10.1021/ie50474a011

Ervin, G. (1977). Solar heat storage using chemical reactions. *Journal of Solid State Chemistry*, *22*(1), 51–61. https://doi.org/10.1016/0022-4596(77)90188-8

Fahim, M. A., & Ford, J. D. (1983). Energy storage using the BaO2-BaO reaction cycle. *The Chemical Engineering Journal*, *27*(1), 21–28. https://doi.org/10.1016/0300-9467(83)80042-2

Fedders, H. et al. (1975). Experiments for combining nuclear heat with the methane steam-reforming process. *Nuclear Engineering and Design*, *34*(1), 119–127. https://doi.org/10.1016/0029-5493(75)90161-2

Fedders, H., & Höhlein, B. (1982). Operating a pilot plant circuit for energy transport with hydrogen-rich gas. *International Journal of Hydrogen Energy*, *7*(10), 793–800. https://doi.org/10.1016/0360-3199(82)90070-2

Felderhoff, M., & Bogdanović, B. (2009). High Temperature Metal Hydrides as Heat Storage Materials for Solar and Related Applications. *International Journal of Molecular Sciences*, *10*(1), 325–344. https://doi.org/10.3390/ijms10010325

Feldhoff, J. F. (2012, June). *Direct Steam Generation (DSG) - Technology Overview*. Presented at the SFERA Summer School 2012, Spain.

Gao, W. et al. (1999). Solubilities of Nitrogen in Selected Naphthenic and Aromatic Hydrocarbons at Temperatures from 344 to 433 K and Pressures to 22.8 MPa. *Journal of Chemical & Engineering Data*, *44*(2), 185–189. https://doi.org/10.1021/je980187y

Garg HP et al. (1985). *Solar Thermal Energy Storage*. Dordrecht, Holland: Reidel Publishing Company.

Ghouse, J. H., & Adams, T. A. (2013). A multi-scale dynamic two-dimensional heterogeneous model for catalytic steam methane reforming reactors. *International Journal of Hydrogen Energy*, *38*(24), 9984–9999. https://doi.org/10.1016/j.ijhydene.2013.05.170

Gil, A. et al. (2010). State of the art on high temperature thermal energy storage for power generation. Part 1—Concepts, materials and modellization. *Renewable and Sustainable Energy Reviews*, *14*(1), 31–55. https://doi.org/10.1016/j.rser.2009.07.035

Haar, L. (1984). *Nbs/Nrc Steam Tables*. CRC Press.

Harper, C. A. (2006). *Handbook of plastics technologies: the complete guide to properties and performance*. McGraw-Hill.

Haynes, W. M. (2010). *CRC Handbook of Chemistry and Physics, 91st Edition*. Taylor & Francis.

Hodoshima, S. et al. (2003). Catalytic decalin dehydrogenation/naphthalene hydrogenation pair as a hydrogen source for fuel-cell vehicle. *International Journal of Hydrogen Energy*, *28*(11), 1255–1262. https://doi.org/10.1016/S0360-3199(02)00250-1

Hodoshima, S. et al. (2005). Hydrogen storage by decalin/naphthalene pair and hydrogen supply to fuel cells by use of superheated liquid-film-type catalysis. *Applied Catalysis A: General*, *283*(1), 235–242. https://doi.org/10.1016/j.apcata.2005.01.010

Huang, T.-C., & Kang, B.-C. (1995). Kinetic Study of Naphthalene Hydrogenation over Pt/Al2O3 Catalyst. *Industrial & Engineering Chemistry Research*, *34*(4), 1140–1148. https://doi.org/10.1021/ie00043a016

IESO. (2016). IESO Home. Retrieved November 1, 2016, from http://www.ieso.ca/

Incropera, F. P. et al. (2011). *Introduction to Heat Transfer* (6th ed.). Wiley and Sons.

Kato, Y. et al. (1999). Durability characteristics of the hydration of magnesium oxide under repetitive reaction. *Journal of Materials Science*, *34*(3), 475–480. https://doi.org/10.1023/A:1004530309298

Kato, Yukitaka et al. (1996). Kinetic study of the hydration of magnesium oxide for a chemical heat pump. *Applied Thermal Engineering*, *16*(11), 853–862. https://doi.org/10.1016/1359-4311(96)00009-9

Kato, Yukitaka et al. (2001). Thermal analysis of a magnesium oxide/water chemical heat pump for cogeneration. *Applied Thermal Engineering*, *21*(10), 1067–1081. https://doi.org/10.1016/S1359-4311(00)00103-4

Kato, Yukitaka et al. (2009). Study on medium-temperature chemical heat storage using mixed hydroxides. *International Journal of Refrigeration*, *32*(4), 661–666. https://doi.org/10.1016/j.ijrefrig.2009.01.032

Khojasteh Salkuyeh, Y., & Adams, T. A. (2015). A novel polygeneration process to co-produce ethylene and electricity from shale gas with zero CO2 emissions via

methane oxidative coupling. *Energy Conversion and Management*, *92*, 406–420. https://doi.org/10.1016/j.enconman.2014.12.081

Kreetz, H. et al. (2000). Maximizing Thermal Power Output of an Ammonia Synthesis Reactor for a Solar Thermochemical Energy Storage System. *Journal of Solar Energy Engineering*, *123*(2), 75–82. https://doi.org/10.1115/1.1352737

Kreetz, H., & Lovegrove, K. (1999). Theoretical analysis and experimental results of a 1 kWchem ammonia synthesis reactor for a solar thermochemical energy storage system. *Solar Energy*, *67*(4), 287–296. https://doi.org/10.1016/S0038-092X(00)00064-5

Kyaw, K., Matsuda, H., et al. (1996). Applicability of Carbonation/Decarbonation Reactions to High-Temperature Thermal Energy Storage and Temperature Upgrading. *Journal of Chemical Engineering of Japan*, *29*(1), 119–125. https://doi.org/10.1252/jcej.29.119

Kyaw, K., Kanamori, M., et al. (1996). Study of Carbonation Reactions of Ca-Mg Oxides for High Temperature Energy Storage and Heat Transformation. *Journal of Chemical Engineering of Japan*, *29*(1), 112–118. https://doi.org/10.1252/jcej.29.112

Labouret, A., & Villoz, M. (2010). *Solar photovoltaic energy*. Stevenage: Institution of Engineering and Technology.

Lovegrove, K. (1993). Thermodynamic limits on the performance of a solar thermochemical energy storage system. *International Journal of Energy Research*, *17*(9), 817–829. https://doi.org/10.1002/er.4440170904

Lovegrove, K et al. (2004). Developing ammonia based thermochemical energy storage for dish power plants. *Solar Energy*, *76*(1), 331–337. https://doi.org/10.1016/j.solener.2003.07.020

Lovegrove, Keith et al. (1999). A solar-driven ammonia-based thermochemical energy storage system. *Solar Energy*, *67*(4), 309–316. https://doi.org/10.1016/S0038-092X(00)00074-8

Meier, A. et al. (2004). Design and experimental investigation of a horizontal rotary reactor for the solar thermal production of lime. *Energy*, *29*(5), 811–821. https://doi.org/10.1016/S0360-5442(03)00187-7

Miyake, Y. et al. (2007). Stereoisomeric effects on volumetric properties under pressure for the system cis- + trans-decalin. *Fluid Phase Equilibria*, *252*(1–2), 79–87. https://doi.org/10.1016/j.fluid.2006.12.011

Nasir, P. et al. (1981). A novel apparatus for the measurement of the phase and volumetric behavior at high temperatures and pressures and its application to study VLE in the hydrogen-tetralin system. *Fluid Phase Equilibria*, *5*(3), 279–288. https://doi.org/10.1016/0378-3812(80)80061-6

NREL. (2010). NSRDB: 1991- 2010 Update. Retrieved October 20, 2016, from http://rredc.nrel.gov/solar/old_data/nsrdb/1991-2010/

NREL. (2013, January). Concentrating Solar Power Projects - Rice Solar Energy Project | Concentrating Solar Power | NREL. Retrieved August 16, 2017, from https://www.nrel.gov/csp/solarpaces/project_detail.cfm/projectID=61

NREL. (2015a, April). Concentrating Solar Power Projects - Xina Solar One | Concentrating Solar Power | NREL. Retrieved August 17, 2017, from https://www.nrel.gov/csp/solarpaces/project_detail.cfm/projectID=275

NREL. (2015b, July). Concentrating Solar Power Projects - Atacama-1 | Concentrating Solar Power | NREL. Retrieved August 17, 2017, from https://www.nrel.gov/csp/solarpaces/project_detail.cfm/projectID=3275

NREL. (2015c, August). Concentrating Solar Power Projects - Solana Generating Station | Concentrating Solar Power | NREL. Retrieved January 27, 2017, from https://www.nrel.gov/csp/solarpaces/project_detail.cfm/projectID=23

NREL. (2016a, February). Concentrating Solar Power Projects - Golmud | Concentrating Solar Power | NREL. Retrieved August 17, 2017, from https://www.nrel.gov/csp/solarpaces/project_detail.cfm/projectID=4301

NREL. (2016b, March). Concentrating Solar Power Projects - Crescent Dunes Solar Energy Project | Concentrating Solar Power | NREL. Retrieved August 16, 2017, from https://www.nrel.gov/csp/solarpaces/project_detail.cfm/projectID=60

NREL. (2016c, June). Concentrating Solar Power Projects - Kathu Solar Park | Concentrating Solar Power | NREL. Retrieved August 17, 2017, from https://www.nrel.gov/csp/solarpaces/project_detail.cfm/projectID=4290

NREL. (2017a, March). Concentrating Solar Power Projects - NOOR I | Concentrating Solar Power | NREL. Retrieved August 17, 2017, from https://www.nrel.gov/csp/solarpaces/project_detail.cfm/projectID=270

NREL. (2017b, April). Concentrating Solar Power Projects - Delingha 50MW Thermal Oil Parabolic Trough project | Concentrating Solar Power | NREL. Retrieved August 17, 2017, from https://www.nrel.gov/csp/solarpaces/project_detail.cfm/projectID=4294

Nur Energie Ltd. (2010, 2017). Tu Nur - Overview -. Retrieved August 16, 2017, from http://www.nurenergie.com/tunur/index.php/english/project/overview

Pardo, P. et al. (2014). A review on high temperature thermochemical heat energy storage. *Renewable and Sustainable Energy Reviews*, *32*, 591–610. https://doi.org/10.1016/j.rser.2013.12.014

Park, J. et al. (1996). Solubilities of Hydrogen in Aromatic Hydrocarbons from 323 to 433 K and Pressures to 21.7 MPa. *Journal of Chemical & Engineering Data*, *41*(1), 70–73. https://doi.org/10.1021/je950152n

Peltier, 12/01/2014 | Dr Robert, & PE. (2014, December 1). Top Plant: Solana Generating Station, Maricopa County, Arizona. Retrieved July 28, 2017, from http://www.powermag.com/solana-generating-station-maricopa-county-arizona/

Perry, R., & Green, D. (2008). *Perry's Chemical Engineers' Handbook, Eighth Edition*. McGraw-Hill Education.

Peters, M. S., & Timmerhaus, K. D. (1991). *Plant design and economics for chemical engineers*. McGraw-Hill.

Rackett, H. G. (1970). Equation of state for saturated liquids. *Journal of Chemical & Engineering Data*, *15*(4), 514–517. https://doi.org/10.1021/je60047a012

Rahimpour, M. R. et al. (2011a). Differential evolution (DE) strategy for optimization of hydrogen production and utilization in a thermally coupled membrane reactor for decalin dehydrogenation and Fischer–Tropsch synthesis in GTL technology. *International Journal of Hydrogen Energy*, *36*(8), 4917–4933. https://doi.org/10.1016/j.ijhydene.2011.01.061

Rahimpour, M. R. et al. (2011b). Simultaneous hydrogen production and utilization via coupling of Fischer–Tropsch synthesis and decalin dehydrogenation reactions in GTL technology. *International Journal of Hydrogen Energy*, *36*(4), 2992–3006. https://doi.org/10.1016/j.ijhydene.2010.11.099

R.C Reid et al. (1987). *The Properties of Gases and Liquids* (4th ed.). New York: McGraw-Hill.

Sakintuna, B. et al. (2007). Metal hydride materials for solid hydrogen storage: A review. *International Journal of Hydrogen Energy*, *32*(9), 1121–1140. https://doi.org/10.1016/j.ijhydene.2006.11.022

Sanz-Bermejo, J. et al. (2014). Comparative System Performance Analysis of Direct Steam Generation Central Receiver Solar Thermal Power Plants in Megawatt Range. *Journal of Solar Energy Engineering*, *136*(1), 010908-010908-9. https://doi.org/10.1115/1.4026279

Sebastián, D. et al. (2008). Hydrogen storage by decalin dehydrogenation/naphthalene hydrogenation pair over platinum catalysts supported on activated carbon. *International Journal of Hydrogen Energy*, *33*(4), 1329–1334. https://doi.org/10.1016/j.ijhydene.2007.12.037

Smith, J. M. 1916-. (1981). *Chemical engineering kinetics* (3d ed.--). McGraw-Hill,.

Stanmore, B. R., & Gilot, P. (2005). Review—calcination and carbonation of limestone during thermal cycling for CO2 sequestration. *Fuel Processing Technology*, *86*(16), 1707–1743. https://doi.org/10.1016/j.fuproc.2005.01.023

Tooley, M., & Dingle, L. (2013). *Engineering Science: For Foundation Degree and Higher National*. Routledge.

U.S. Department of Energy. (2014). *2014: The Year of Concentrating Solar Power*.

U.S. Department of Energy. (2017a). Electricity data browser - Solana Generating Station. Retrieved February 21, 2017, from https://www.eia.gov/electricity/data/browser/#/plant/56812

U.S. Department of Energy. (2017b). Hydrogen Storage | Department of Energy. Retrieved August 16, 2017, from https://energy.gov/eere/fuelcells/hydrogen-storage

Valenzuela, L. et al. (2004). Direct steam generation in solar boilers. *Control Systems Magazine, IEEE*, *24*(2), 15–29.

Wakao, N. (1982). *Heat and mass transfer in packed beds*. Gordon and Breach Science Publishers,.

Wang, B. et al. (2008). Kinetic modeling of pure hydrogen production from decalin. *Journal of Catalysis*, *253*(2), 229–238. https://doi.org/10.1016/j.jcat.2007.11.012

Wentworth, W. E., & Chen, E. (1976). Simple thermal decomposition reactions for storage of solar thermal energy. *Solar Energy*, *18*(3), 205–214. https://doi.org/10.1016/0038-092X(76)90019-0

Wörner, A., & Tamme, R. (1998). CO2 reforming of methane in a solar driven volumetric receiver–reactor. *Catalysis Today*, *46*(2), 165–174. https://doi.org/10.1016/S0920-5861(98)00338-1

Zhang, H. L. et al. (2013). Concentrated solar power plants: Review and design methodology. *Renewable and Sustainable Energy Reviews*, *22*, 466–481. https://doi.org/10.1016/j.rser.2013.01.032